A&A 493, 425–444 (2009)
DOI: 10.1051/0004-6361:20066907

Astronomy & Astrophysics

Absorption line indices in the *UV*

I. Empirical and theoretical stellar population models

C. Maraston[1], L. Nieves Colmenárez[2], R. Bender[2,3], and D. Thomas[1]

[1] University of Portsmouth, Dennis Sciama Building, Burnaby Road, Portsmouth, PO1 3QL, UK
e-mail: claudia.maraston@port.ac.uk
[2] Max-Planck-Institute für extraterrestrische Physik, Giessenbachstr. 1, 85741 Garching, Germany
[3] Universitäts-Sternwarte München, Scheinerstr. 1, 81679 München, Germany

Received 8 December 2006 / Accepted 13 September 2008

ABSTRACT

Aims. Stellar absorption lines in the optical (e.g. the Lick system) have been extensively studied and constitute an important stellar population diagnostic for galaxies in the local universe and up to moderate redshifts. Proceeding towards higher look-back times, galaxies are younger and the ultraviolet becomes the relevant spectral region where the dominant stellar populations shine. A comprehensive study of ultraviolet absorption lines of stellar population models is however still lacking. With this in mind, we study absorption line indices in the far and mid-ultraviolet in order to determine age and metallicity indicators for *UV*-bright stellar populations in the local universe as well as at high redshift.

Methods. We explore empirical and theoretical spectral libraries and use evolutionary population synthesis to compute synthetic line indices of stellar population models. From the empirical side, we exploit the IUE-low resolution library of stellar spectra and system of absorption lines, from which we derive analytical functions (fitting functions) describing the strength of stellar line indices as a function of gravity, temperature and metallicity. The fitting functions are entered into an evolutionary population synthesis code in order to compute the integrated line indices of stellar populations models. The same line indices are also directly evaluated on theoretical spectral energy distributions of stellar population models based on Kurucz high-resolution synthetic spectra, In order to select indices that can be used as age and/or metallicity indicators for distant galaxies and globular clusters, we compare the models to data of template globular clusters from the Magellanic Clouds with independently known ages and metallicities.

Results. We provide synthetic line indices in the wavelength range ∼1200 Å to ∼3000 Å for stellar populations of various ages and metallicities.This adds several new indices to the already well-studied CIV and SiIV absorptions. Based on the comparison with globular cluster data, we select a set of 11 indices blueward of the 2000 Å rest-frame that allows us to recover well the ages and the metallicities of the clusters. These indices are ideal to study ages and metallicities of young galaxies at high redshift. We also provide the synthetic high-resolution stellar population SEDs.

Key words. galaxies: evolution – galaxies: stellar content – galaxies: star clusters – galaxies: Magellanic Clouds

1. Introduction

The far and mid-ultraviolet region of the electromagnetic spectrum ($\lambda \sim$ 1200−3200 Å) traces the hot component of galaxy stellar populations, that in young galaxies is made up of luminous O and B-type stars. These leave a characteristic imprint in the integrated spectra in the form of numerous absorption features, related to key chemical species like silicon, carbon, iron, magnesium, etc. Old stellar populations can also produce a hot stellar component if sufficient mass-loss occurs, as shown by well-known phenomena such as the extreme blue horizontal branch in globular clusters (e.g. de Boer 1985) and the *UV*-upturn of elliptical galaxies (e.g. Dorman et al. 1995; Burstein et al. 1988; Greggio & Renzini 1990). In this first paper we focus on young and massive stars as producers of *UV* light.

Thanks to substantial improvement in observational capabilities, it is now feasible to obtain the rest-frame ultraviolet spectrum of galaxies up to very high redshift (see e.g., Yee et al. 1996; Steidel et al. 1996; Pettini et al. 2000; Mehlert et al. 2001; de Mello et al. 2004; Cimatti et al. 2004; McCarthy et al. 2004; Daddi et al. 2005; Popesso et al. 2008). From the modelling side, extensive work is being invested in understanding the intrinsic *UV* spectrum of young stellar populations as a function of their basic parameters – age, metallicity, star formation history and Initial Mass Function – (Robert et al. 1993; Leitherer & Lamers 1991; Leitherer & Heckman 1995; Leitherer et al. 1999, hereafter SB99; de Mello et al. 2000). In these works, the *UV* spectra of stellar populations are obtained by using observed stellar spectra of O, B stars in the Milky Way and Magellanic Clouds, or synthetic spectra derived from model atmospheres. Rix et al. (2004) have used high-resolution *UV* theoretical stellar spectra (Pauldrach et al. 2001), in order to extend the modelling to sub-solar and super-solar metallicities. This work focuses on the Si IV and C IV lines that are the most prominent absorption features in the *UV*. A well-known limitation imposed by the use of empirical libraries is the narrow metallicity range spanned by the real stars – usually not too different from solar. On the other hand, a clear advantage of using real stars is that the empirical spectra should contain the effect of stellar winds that affect the photospheric lines of massive stars and are complicated to model (e.g. Kudritzki et al. 1987).

In this work we take a complementary approach to existing models. We follow a twofold strategy and compute both empirically-based models as well as theoretical ones.

Table 1. Definition of the absorption index system (F92).

N	Name	Blue bandpass		Central bandpass		Red bandpass		Comments
(1)	(2)	(3)	(4)	(5)	(6)	(7)	(8)	(9)
1	BL_{1302}	1270.0	1290.0	1292.0	1312.0	1345.0	1365.0	Si III, Si II, O I
2	Si IV	1345.0	1365.0	1387.0	1407.0	1475.0	1495.0	Si IV 1393.8; 1402.8
3	BL_{1425}	1345.0	1365.0	1415.0	1435.0	1475.0	1495.0	C II 1429, Si III 1417, Fe IV, Fe V
4	Fe 1453	1345.0	1365.0	1440.0	1466.0	1475.0	1495.0	Fe V +20 additional Fe lines
5	C^A_{IV}	1500.0	1520.0	1530.0	1550.0	1577.0	1597.0	C IV 1548, in absorption
6	C IV	1500.0	1520.0	1540.0	1560.0	1577.0	1597.0	C IV 1548, central band
7	C^E_{IV}	1500.0	1520.0	1550.0	1570.0	1577.0	1597.0	C IV 1548, in emission.
8	BL_{1617}	1577.0	1597.0	1604.0	1630.0	1685.0	1705.0	Fe IV
9	BL_{1664}	1577.0	1597.0	1651.0	1677.0	1685.0	1705.0	C I 1656.9, Al II 1670.8
10	BL_{1719}	1685.0	1705.0	1709.0	1729.0	1803.0	1823.0	N IV 1718.6, Si IV 1722.5; 1727.4, Al II
11	BL_{1853}	1803.0	1823.0	1838.0	1868.0	1885.0	1915.0	Al II, Al III, Fe II, Fe III
12	Fe II (2402 Å)	2285.0	2325.0	2382.0	2422.0	2432.0	2458.0	
13	BL_{2538}	2432.0	2458.0	2520.0	2556.0	2562.0	2588.0	Uncertain, Fe I?
14	Fe II (2609 Å)	2562.0	2588.0	2596.0	2622.0	2647.0	2673.0	
15	Mg II	2762.0	2782.0	2784.0	2814.0	2818.0	2838.0	
16	Mg I	2818.0	2838.0	2839.0	2865.0	2906.0	2936.0	
17	Mg_{wide}	2470.0	2670.0	2670.0	2870.0	2930.0	3130.0	
18	Fe I	2906.0	2936.0	2965.0	3025.0	3031.0	3051.0	
19	BL_{3096}	3031.0	3051.0	3086.0	3106.0	3115.0	3155.0	Al I 3092, Fe I 3091.6

Columns correspond to: (1) index number; (2) name; (3 and 4) blue passband definition; (5 and 6) central passband definition; (7 and 8) red passband definition; and (9) comments regarding the relevant chemical elements. Indices termed as "BL" are blends of several elements. Adaptation from F92 (see their Tables 3.A and 3.B).

From the empirical side we exploit the full potential of the Fanelli et al. (1992, F92 hereafter) empirical library of *IUE* spectra and index system for population synthesis models.

We construct analytical polynomial fits (fitting functions, FF) that trace the empirical indices as functions of stellar parameters. FF can be easily incorporated into an evolutionary synthesis code in order to predict the integrated indices of stellar populations. Another advantage is that fluctuations in the spectra of stars with similar atmospheric parameters are averaged out. Absorption line indices have the advantage of being insensitive to reddening, which is a serious issue in the *UV* of young stellar populations. This is particularly important for high-redshift studies where little is known about dust reddening. To our knowledge, this is the first work in which the F92 library of stellar groups and index system is thoroughly examined for evolutionary population synthesis studies, although individual indices in the system have been considered in previous works (see e.g.: Fanelli et al. 1988; Ponder et al. 1998; Heap et al. 1998; Lotz et al. 2000).

In parallel, we compute fully theoretical indices by incorporating a high-resolution version of the Kurucz library of stellar spectra (Rodríguez-Merino et al. 2005) in the Maraston (2005) evolutionary population synthesis code.

We compare the models with observations of young star clusters in the Magellanic Clouds. Star clusters with independently known ages and metallicities are in principle the ideal templates for stellar population models and this comparison should give indications on which indices are reliable tracers of ages and metallicities and can be applied with confidence to study distant galaxies. Care has to be taken since spectral lines are also sensitive to specific element ratios of individual elements, which may be the case for some of the indices we study here.

This paper is structured as follows. In Sect. 2 we briefly recall the evolutionary population synthesis code we adopt and its ingredients. In Sect. 3 we summarise the relevant features of the IUE index system and empirical spectral library. Section 4 explains the construction of the fitting functions, their behaviour with changes in stellar atmospheric parameters and how we include metallicity effects. In Sect. 5 we describe the construction of the stellar population models, both empirical and theoretical and in Sect. 6 we test the models with star cluster data. In Sect. 7 we provide a summary and conclusions.

2. Evolutionary population synthesis ingredients

The evolutionary population synthesis (EPS) technique allows the computation of the spectro-photometric properties of stellar populations using stellar evolutionary tracks (Buzzoni 1989; Bruzual & Charlot 1993; Worthey 1994a; Vazdekis et al. 1996; Fioc & Rocca-Volmerange 1997; Maraston 1998; Leitherer et al. 1999; Bruzual & Charlot 2003; Maraston 2005; Schiavon 2007, among others). The main target of EPS models are the stellar populations that cannot be resolved into individual stars. EPS models provide the theoretical framework for interpreting such systems, in particular for deriving ages and chemical abundances.

In this work we use the EPS models and code by Maraston (1998, 2005, hereafter M05), in which the stellar tracks and isochrones are taken from the Geneva database (Schaller et al. 1992; Schaerer et al. 1993) for young ages ($t \lesssim 30$ Myr), and from the Frascati database for older ages (see Table 1 in M05). The evolution of massive stars is affected by (mostly unknown) mass-loss, besides rotation and convective overshooting. Differences exist between the Geneva evolutionary tracks, and, for example, those from the Padova database (e.g. Girardi et al. 2000), especially in the post-Main Sequence evolution. However, *UV* spectral indices, as the *UV* luminosity, mostly depend on the stars around the Main Sequence turnoff, hence the uncertainties in the post-Main Sequence evolution should have a marginal effect. As an example, Fig. 1 shows for a 30 Myr old, $Z_\odot$ simple stellar population SSP (Maraston 1998) the relative contributions from the individual stars to the total luminosity at $\lambda\lambda$1500 Å (left panel) and $\lambda\lambda$2500 Å (right panel), as a function of the effective temperature ($T_{\rm eff}$) and the surface

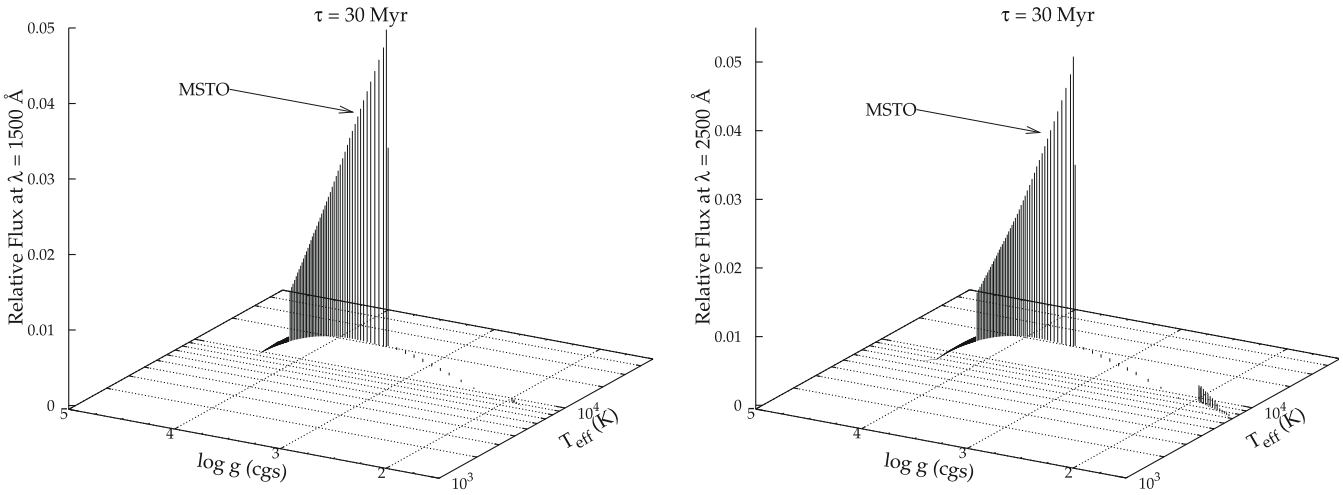

Fig. 1. Contributions to the luminosity at 1500 Å (*left panel*) and 2500 Å (*right panel*), from stars of a 30 Myr old simple stellar population with $Z_\odot$ metallicity (Maraston 1998), as functions of effective temperature $T_{\rm eff}$ and surface gravity $\log g$. Stars around the Main Sequence turnoff contribute the bulk of the luminosity at these wavelengths.

gravity ($\log g$). Stars around the Main Sequence turnoff dominate the emission, contributing more than 90% to the total luminosity. To gain more insight into the effects of stellar tracks, we also evaluate spectral indices using stellar population models based on the Padova tracks (see Sect. 6.5).

3. Spectral library and line index system

We use the library of stellar spectra assembled by F92, from *IUE* low-resolution (6 Å) observations of 218 stars in the solar neighbourhood. Spectra cover the range $\lambda\lambda$1150–3200 Å in wavelength and are compiled in the "IUE Ultraviolet spectral atlas" (Wu et al. 1983, 1991). In its final form, the library consists of 56 mean stellar groups, classified by spectral type (from O3 to M4) and luminosity class (I, III, IV and V). Out of the 56 stellar groups, the 47 groups classified by F92 as having solar metallicity were selected as input for the fitting functions. The "metal-poor" and "metal-rich" groups were excluded, due to their very low number. Each stellar group is constructed by averaging the spectra of a variable number of individual stars (between 2 and 12) with similar spectral types, colours, luminosity classes and when possible direct metallicity determination. When the metallicity was not known, the grouping was made by matching the spectrum. The weight of each spectrum is inversely proportional to the mean signal-to-noise ratio (S/N), measured within a 100 Å line-free window, centred at 2450, 2550 and 2700 Å for spectral types O-G4; G5-K3 and K4-M, respectively (see F92, for more details).

We adopt the line index system defined by Fanelli et al. (1987, 1990, 1992), which comprises 11 indices in the far-*UV* ($\lambda\lambda$1270–1915 Å) and 8 indices in the mid-*UV* ($\lambda\lambda$2285–3130 Å). In Table 1 we recall the index definitions, with their central and bracketing sidebands, and collect relevant comments about the atomic species contributing to the absorption, according to literature identifications (Fanelli et al. 1990; Bonatto et al. 1995; Kinney et al. 1993; Coluzzi 1993). In Fig. 2 we illustrate graphically the index bandpasses on stellar spectra.

3.1. Derivation of stellar parameters $T_{\rm eff}$ and $\log g$

In order to construct analytical approximations which will describe stellar absorption indices as functions of $T_{\rm eff}$ and $\log g$, we need to transform the observed $(B-V, M_V)$ of the groups (from O'Connell 1976; Schmidt-Kaler 1982; Humphreys & McElroy 1984) into the theoretical $(T_{\rm eff}, \log g)$. This is done by superimposing isochrones on the colour magnitude diagram of stellar groups (Fig. 3), and selecting the atmospheric parameters along the isochrones with the closest absolute magnitude and colour. Solar metallicity isochrones from Schaller et al. (1992); Meynet et al. (1994) were used, for consistency with the ingredients of the SSP models. The adopted calibration is given in Table 2.

In order to check that our adopted calibration, that is based on a specific set of isochrones, can be generalised to any arbitrary computation, we have calculated the effective temperatures using a completely independent calibration (by de Jager & Nieuwenhuijzen 1987). The result is reported in Fig. 4a. As can be seen, the two calibrations are consistent, the average absolute difference in effective temperature being small, $\langle|\log T_{\rm eff}^{\rm Gen} - \log T_{\rm eff}^{\rm JN87}|\rangle = 0.02$ dex. We have also checked that the corresponding effect on the FFs leaves the stellar population models basically unchanged.

What F92 call the "solar" groups actually include stars with a spread in metallicity, and even stars for which there were no spectroscopic metallicity determinations, and the metallicity was assigned by visual inspection of the spectra and spectrum matching. We have checked whether the metallicity so determined agrees with other, more recent, estimates. We did the exercise for roughly half the sample (96 out of 189 stars). Figure 4b shows the result, in which the F92 metallicity is plotted versus the values from the Cayrel de Strobel et al. (1997) and other catalogues (Wallerstein & Helfer 1959; Helfer et al. 1960; Parker et al. 1961; Wallerstein 1962; Bell & Rodgers 1965; Conti et al. 1965; Alexander 1967; Cayrel de Strobel et al. 1970; Chaffee et al. 1971; Hearnshaw 1974; Tomkin & Lambert 1978; Luck 1979; Luck & Lambert 1981; Cayrel et al. 1985; Boesgaard 1989; Boesgaard & Friel 1990; Cayrel de Strobel et al. 1997). There is no clear bias in the metallicity determination of F92. This is the case even for the stars for which F92 did not have a metallicity determination at the time of assembly of the library (the vertical group of stars at [Fe/H] = 0), as outliers are found to be evenly divided between sub and super-solar metallicity. Finally, and reassuringly, the tail of stars that were included by F92 in the solar group though they were assigned super-solar metallicity at the

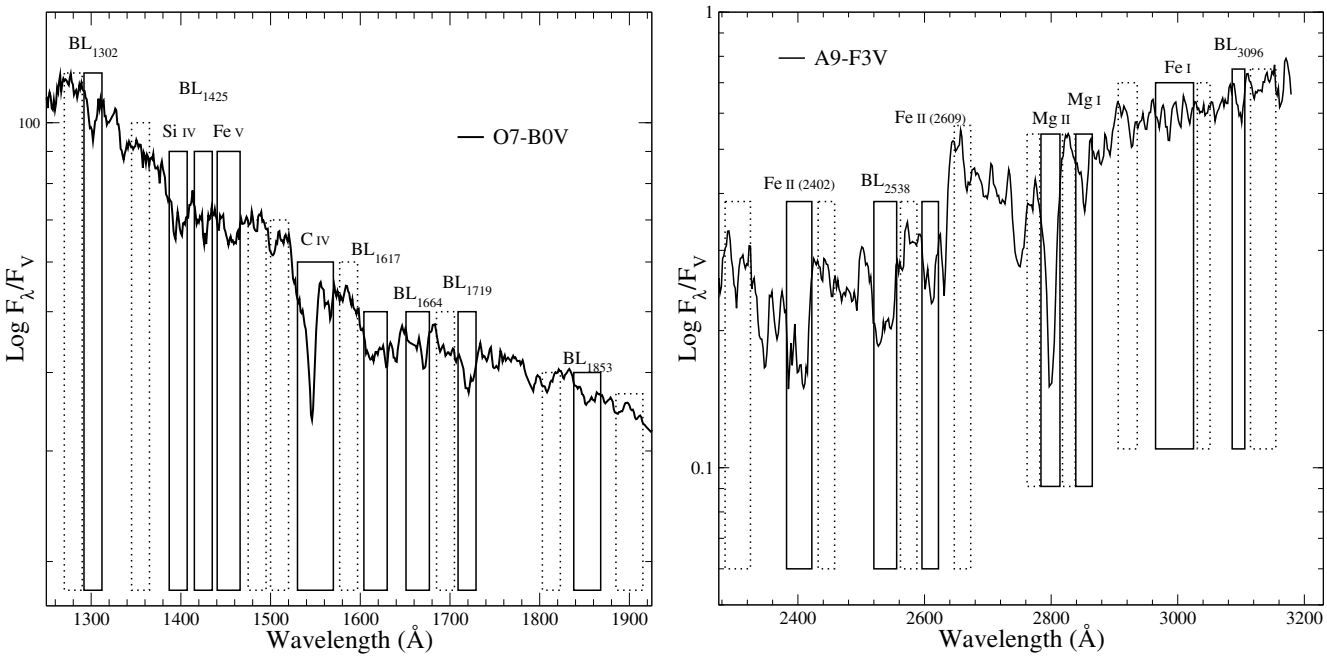

Fig. 2. Visualisation of index bandpasses on representative stellar spectra. *The left-hand panel* shows the far-*UV* indices with the central bandpasses highlighted by solid boxes and the blue and red continuum bandpasses marked by dotted boxes. *The right-hand panel* shows, in the same way, the mid-*UV* indices. The bandpasses for the Mg_{wide} index are not depicted in order to avoid crowding.

time are found through the new determinations to indeed have metallicities around solar.

3.2. Line indices and errors for stellar groups

The *UV* line indices defined by F92 are expressed as equivalent widths and given in Å. We measure them on the empirical spectra of each group, following standard definitions (Burstein et al. 1984; Faber et al. 1985):

$$EW_{\lambda_{i,f}} = \int_{\lambda_i}^{\lambda_f} \left(1 - \frac{S(\lambda)}{C(\lambda)}\right) \mathrm{d}\lambda \quad (1)$$

where $S(\lambda)$ and $C(\lambda)$ are the fluxes in the line and in the continuum, respectively. The statistical errors in the equivalent width are computed following Cardiel et al. (1998):

$$\sigma^2_{EW} = \left(\sum_{i=1}^{N}\left[\frac{C^2(\lambda_i)\sigma_i^2 + S^2(\lambda_i)\sigma^2_{C(\lambda_i)}}{C^4(\lambda_i)}\right] + \sum_{i=1}^{N}\sum_{j=1,j\neq i}^{N}\left[\frac{S(\lambda_i)S(\lambda_j)}{C^2(\lambda_i)C^2(\lambda_j)}(\Lambda_1\sigma^2_{\rm B} + \Lambda_4\sigma^2_{\rm R})\right]\right)\Delta. \quad (2)$$

In Eq. (2) $S(\lambda_i)$, σ_i and $C(\lambda_i)$, $\sigma_{C(\lambda_i)}$ are the fluxes and dispersions in the line and in the pseudo-continua respectively, Δ is the pixel size, $\sigma_{\rm B}$ and $\sigma_{\rm R}$ are the dispersions in the mean fluxes within the blue and red band-passes respectively. The parameters $\Lambda_{1,4}$ are defined as:

$$\Lambda_1 = \frac{(\lambda_{\rm R} - \lambda_i)(\lambda_{\rm R} - \lambda_j)}{(\lambda_{\rm R} - \lambda_{\rm B})^2} \quad (3)$$

$$\Lambda_4 = \frac{(\lambda_i - \lambda_{\rm B})(\lambda_j - \lambda_{\rm B})}{(\lambda_{\rm R} - \lambda_{\rm B})^2} \quad (4)$$

where $\lambda_{\rm B}$ and $\lambda_{\rm R}$ are the central wavelengths of the blue and red band-pasess, respectively.

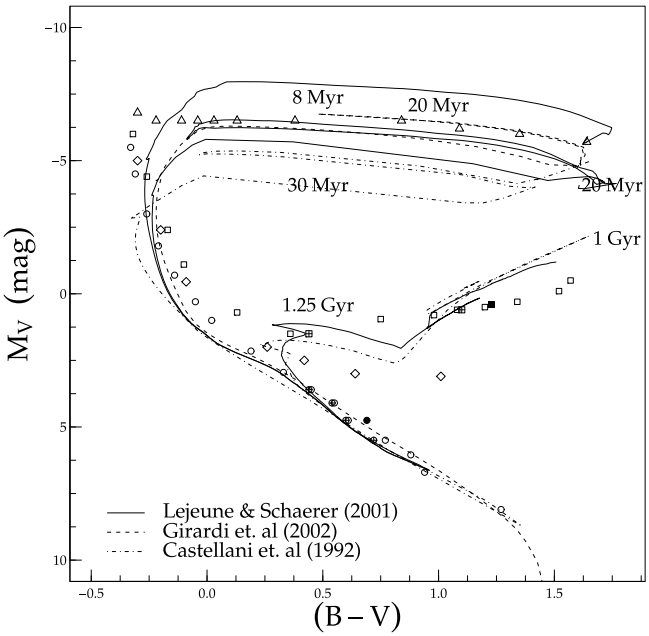

Fig. 3. CMD of the stellar groups in the F92 library. Different symbols are used to denote the different luminosity classes, dwarfs (V, circles), giants (III, squares), sub-giants (IV, diamonds) and super-giants (I and II, triangles). Different fill styles correspond to different metallicities, solar (empty), sub-solar (crossed) and super-solar (black-filled). Isochrones of 8, 20 Myr and 1.25 Gyr (thick curve, from the compilation of Lejeune & Schaerer 2001), with 20 Myr (dashed curve, from Girardi et al. (2002) and 30 Myr and 1 Gyr (dot-dashed curve, from Castellani et al. (1992) are superimposed to highlight the coverage of the library in terms of stellar population parameters. All isochrones have solar metallicity.

The dispersion σ_i is assumed to be proportional, at each wavelength, to the mean fractional dispersion $\langle Q \rangle$ defined by

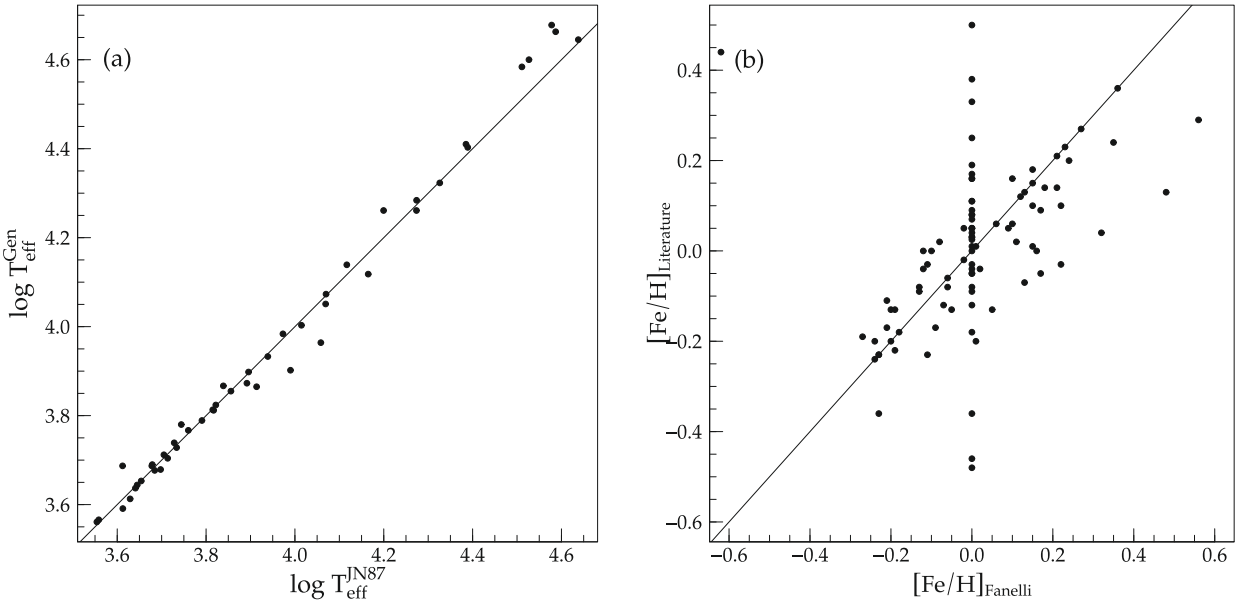

Fig. 4. a) Comparison of $T_{\rm eff}$ calibrations derived with two different methods. The y-axis represents effective temperatures derived from superposition of Geneva Group isochrones, while the x-axis represents effective temperatures derived by interpolation of the de Jager & Nieuwenhuijzen (1987) tables. The solid line represents the one-to-one correlation. **b)** Metallicity of individual stars used to build the "solar metallicity" stellar groups in the F92 library, compared to metallicity determinations found in the literature.

Table 2. Adopted transformation from the observational spectral type (through $B-V, M_V$) to the theoretical plane $T_{\rm eff}, \log g$. Based on isochrones from Schaller et al. (1992); Meynet et al. (1994).

Group	$T_{\rm eff}$ (K)	$\log g$ (cgs)	Group	$T_{\rm eff}$ (K)	$\log g$ (cgs)
O3-6V	44 157	4.045	B0-2III	25 293	3.517
O7-B0V	39 811	4.106	B3-6III	18 239	3.719
B1-1.5V	25 704	3.961	B7-9III	11 246	3.617
B2-4V	19 231	3.972	A3-6III	8570	3.855
B5-8V	13 772	3.959	A9-F6III	7362	3.856
B9-9.5V	10 069	3.939	G0-5III	5058	2.942
A0-2V	9638	4.113	G5-K0III	4753	2.706
A5-8V	7907	4.196	K0-2III	4498	2.376
A9-F3V	7161	4.278	K2III	4335	2.163
F5-7V	6501	4.279	K3III	4102	1.787
F8-9V	6152	4.320	K4-5III	3899	1.403
G0-5V	5848	4.419	K7-M3III	3681	0.977
G6-9V	5483	4.541	O4-9I	47 643	3.913
K0-1V	5152	4.597	B0-2I	21 038	2.733
K2-3V	4864	4.656	B3-5I	13 122	2.196
K5-M0V	4864	4.656	B6-9I	9204	1.742
O9-B0IV	38 371	3.921	A0-2I	7980	1.576
B2-5IV	18 239	3.719	A5-F0I	7328	1.426
B8-9IV	11 830	3.877	F2-8I	6486	1.217
A7-F0IV	7464	4.044	G0-3I	5346	0.820
F2-7IV	6668	3.982	G5-8I	4775	0.666
G0-2IV	6026	3.926	K2-3I	4406	0.515
G8-K1IV	4898	3.437	K5-M4I	3639	–0.164
O5-6III	46 026	4.004			

F92 for each stellar group. The dispersions of the pseudo-continuum flux $\sigma_{C(\lambda_i)}$ and of the mean fluxes in the blue and red passbands $\sigma_{\rm B}$ and $\sigma_{\rm R}$ are calculated by error propagation. We refer to Cardiel et al. (1998) for more details.

4. Fitting functions

Our main objective is to study the behaviour of integrated *UV* absorption line indices of stellar population models, as functions of the stellar population parameters age (t) and metallicity ([Z/H]). In order to include an empirical calibration in an evolutionary population synthesis code, one convenient approach followed by many authors is the construction of analytical approximations that describe the empirical line indices as functions of stellar parameters ($T_{\rm eff}$, $\log g$, [Z/H]) (fitting functions, FF, e.g. Buzzoni et al. 1992; Gorgas et al. 1993; Worthey et al. 1994; Cenarro et al. 2002; Schiavon 2007).

We adopt the FF approach because FF can be easily incorporated into an evolutionary synthesis code in order to predict the integrated indices of stellar populations. Another advantage is that fluctuations in the spectra of stars with similar atmospheric parameters become averaged out.

Since the observed stars have mostly solar chemical composition as a first step we build FFs that depend only on $T_{\rm eff}$ and $\log g$. We then incorporate metallicity effects by means of synthetic spectra (Sect. 4.2).

It is important to point out that the specific ratios of various elements in this sample of stars may dominate the index values similarly to what has been found for optical lines (e.g., Burstein et al. 1984; Worthey et al. 1992; Thomas et al. 2003) and this is a fact that one must bear in mind when the models are compared to extragalactic stellar populations. In this work we do not perform an element-ratio-sensitive modelling, which will be the subject of a future study.

For the analytical form of the FFs we chose polynomials because these are the simplest functions, including, in principle all possible terms (20 in total):

$$EW = \phi(\log T_{\rm eff}, \log g) = \sum_{i=0}^{3} \sum_{j=0}^{i} a_{ij} \log T_{\rm eff}^{i} \log g^{j}. \quad (5)$$

In practice, in several cases it was not possible to accurately reproduce the index behaviour using only one function of the form given by Eq. (5). In these cases we split the temperature range into two regions (the "cool" region between effective temperatures T_{a_1} and T_{a_2}, and the "hot" region between effective

temperatures T_{b_1} and T_{b_2}) inside which the fitting procedure was carried out independently. Both regions are chosen to overlap and share several stellar groups in common. If $\phi_a(\log T_{\rm eff}, \log g)$ and $\phi_b(\log T_{\rm eff}, \log g)$ are the local FFs corresponding to the first and the second region, defined respectively in the intervals $\log T_{\rm eff} \in [T_{a_1}, T_{a_2}]$ and $\log T_{\rm eff} \in [T_{b_1}, T_{b_2}]$ (with $T_{b_1} < T_{a_2}$), the interpolated FF $\phi_{ab}(\log T_{\rm eff}, \log g)$ is defined as (Cenarro et al. 2002):

$$\phi_{ab}(\log T_{\rm eff}, \log g) = \omega\phi_a(\log T_{\rm eff}, \log g) + (1-\omega)\phi_b(\log T_{\rm eff}, \log g) \quad (6)$$

where ω is the weighting factor and is defined as:

$$\omega = \cos^2\left(\frac{\pi}{2}\frac{\log T_{\rm eff} - \log T_{b_1}}{\log T_{a_2} - \log T_{b_1}}\right). \quad (7)$$

The continuity of the FF is ensured by imposing that $\phi_{ab}(T_{a_2}, \log g) = \phi_b(T_{a_2}, \log g)$ and that $\phi_{ab}(T_{b_1}, \log g) = \phi_a(T_{b_1}, \log g)$.

The polynomial coefficients a_{ij} are computed through iterative linear fitting, discarding in each step the statistically least significant coefficients. These are determined by their p-value, which is the probability that the true coefficient has a value greater than or equal to the computed one strictly by chance. We consider as significant coefficients those with a p-value less than or equal to 5%. The fitting is recomputed after dropping the non-significant coefficients and the statistical significance of the remaining coefficients is re-evaluated. The procedure stops once all coefficients are statistically significant.

The choice of the limits defining the two regions where local FFs are computed is arbitrary, therefore the best combination is found by trial and error, evaluating the effectiveness of the FFs in describing the global index behaviour. An important parameter we take into account is the lack of evident trends in the distribution of the residuals. In the case of existence of such trends, the local limits were re-adjusted or we inspected the individual group's spectra in order to understand if the deviations are due to particular features in them.

For each index the best fit parameters are provided together with the validity ranges ($3.6 \lesssim T_{\rm eff}/{\rm kK} \lesssim 47.5$; and $-0.1 \lesssim \log g \lesssim 4.66$), which are fundamental to avoid the raising of spurious results as a product of extrapolating the FFs outside the limits in which they where derived and inside which the statistical significance is guaranteed (see Maraston et al. 2003, for a discussion on this issue and examples).

4.1. Summary of index behaviour with stellar parameters

The trends of the various line indices in the IUE sample stars as functions of the stellar parameters $T_{\rm eff}$, $\log g$ and metallicity is discussed in detail by Massa (1989); Walborn & Panek (1984); Fanelli et al. (1987); F92. Some of the mid-*UV* indices by Fanelli et al. have also been studied in theoretical Kurucz stellar spectra by Chavez et al. (2007).

Below we summarise the relevant conclusions from these works.

In the far *UV* the most prominent absorption features are BL_{1302}, BL_{1664}, Si IV (1400 Å) and C IV (1550 Å).

BL_{1302} is a blend of several O I (1302.704, 1304.858, 1306.023 Å), Si III (1298.90, 1303.30 Å) and Si II (1304.41 Å) (Coluzzi 1993; F92; Moore 1952) lines. It reaches a maximum for late B stars, decreasing with increasing temperature, with very little dependence on gravity. Similarly, Si IV and C IV reach maxima around early B – late O spectral types, but show a stronger gravity dependence. BL_{1425} is a blend of several Fe V, C III and Si III lines; it reaches a maximum for early B spectral types (~30 kK), but its temperature dependence is very weak. The blend of Fe V lines at 1453 Å shows instead a stronger temperature dependence, with early O stars displaying the highest equivalent widths and practically vanishing for mid to late B stars. BL_{1617} is a blend of Fe IV and Fe V lines, which is strongest for mid O stars. BL_{1664} already shows the behaviour typical of mid-*UV* absorption indices. It measures the combined absorption by the resonant lines of Al II (1670.8 Å) and C I (1656.9 Å). It increases monotonously from spectral types around B5 up to early A starts ($T_{\rm eff} \sim 10$ kK). BL_{1719} is a blend of N IV (1718.6 Å), Si IV (1722.5 Å) and several Fe IV multiplets. It shows a remarkable lack of temperature sensitivity, which was observed first by Underhill et al. (1972), and a mild surface gravity dependence. The last among the far-*UV* indices is BL_{1853}, a blend of several Fe II, Al II and Al III transitions. Its behaviour is similar to that of BL_{1664}, with a strong increase for spectral types cooler than A0 ($T_{\rm eff} \sim 10$ kK), but with better surface gravity separation.

In the mid-*UV*, the most prominent absorptions features are the Mg II 2800 Å, the Fe I 3000 Å which trace four neutral magnesium lines (2966.901; 2984.7302; 2999.8092 and 3021.37049 Å), the two iron Fe II features at 2402 and 2609 Å and Mg I at 2852 Å, respectively. These indices show the same qualitative behaviour, being close to zero until late B spectral types, then increasing towards earlier types reaching maxima around late F and early G spectral type stars. The magnesium Mg II 2800 Å shows some peculiar behaviour as a function of metallicity (Fanelli et al. 1990), and we postpone its discussion to Sect. 6.3. BL_{2538} is a blend of Fe I and Mg I which starts to rise strongly for stars cooler than early A-type and reaches its maximum at late F stars ($T_{\rm eff} \sim 6$ kK), with a very clear gravity segregation (dwarfs have equivalent widths nearly twice as high as supergiants at the peak). A similar luminosity-class separation is displayed by Fe II 2402 and Fe I 3000. BL_{3096}, a blend of Fe I and Al I lines, does not reach a maximum in our explored parameter space, showing a monotonic increase with decreasing temperature.

In Fig. 5 we show the fitting functions as a function of temperature for different gravities, overlaid on the data of the individual stars used in the fits. Coefficients of the polynomials are provided in the Appendix.

In Sect. 6.5, we compare our FF-based models with other models using the Fanelli et al. library directly and find that the results are consistent. This indicates that the fitting function procedure has not introduced spurious effects.

4.2. Inclusion of metallicity effects

As shown in Fig. 4b, the spectral library of F92 is mostly composed of stars of solar metallicity. On the other hand, the consideration of metallicity effects on the integrated spectrophotometric properties of stellar populations is very important, as it allows us to gain insights into the galaxy formation process and the global star formation history of the universe.

In order to include the dependence on metallicity in the FFs we use the library of high-resolution synthetic Kurucz spectra calculated by Rodríguez-Merino et al. (2005) (see Sect. 5).

We consider model spectra with $\log g = 4$, since the most important contributors to the *UV* light are turnoff stars and gravity does not vary appreciably around the Main Sequence turnoff.

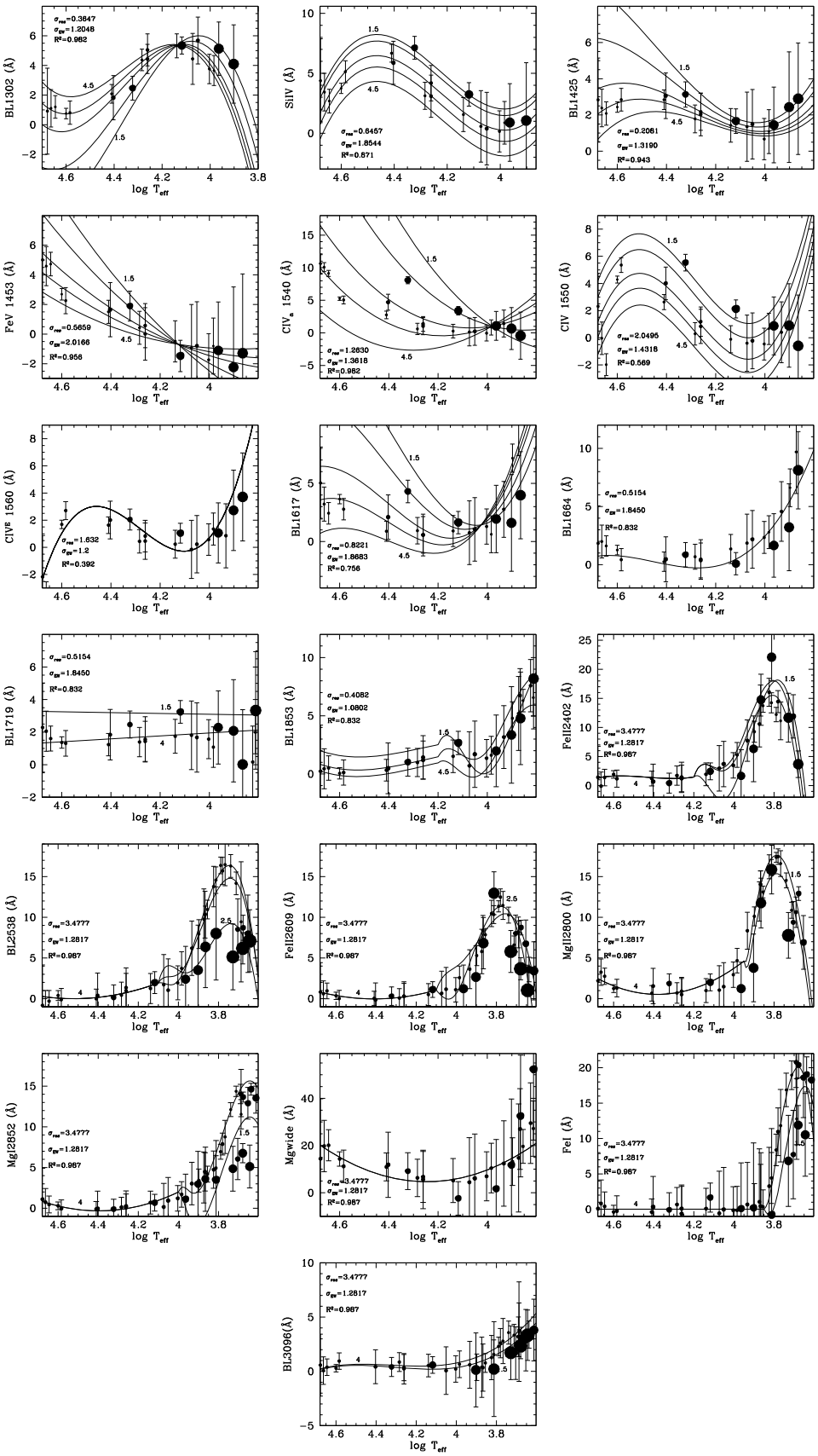

Fig. 5. Fitting functions. Stellar *EW*s are shown as functions of the effective temperature. The surface gravity is encoded in the symbol size (large circles for giants, small circles for dwarfs), using a linear function with a slope of 2.6 and a zero-point of 0.8. FFs for various gravities (see labels) are plotted. The standard deviation of the residuals ($\sigma_{\rm res}$) and the mean equivalent width error $\overline{\sigma_{\rm W}}$ of all the groups included the fit are also shown.

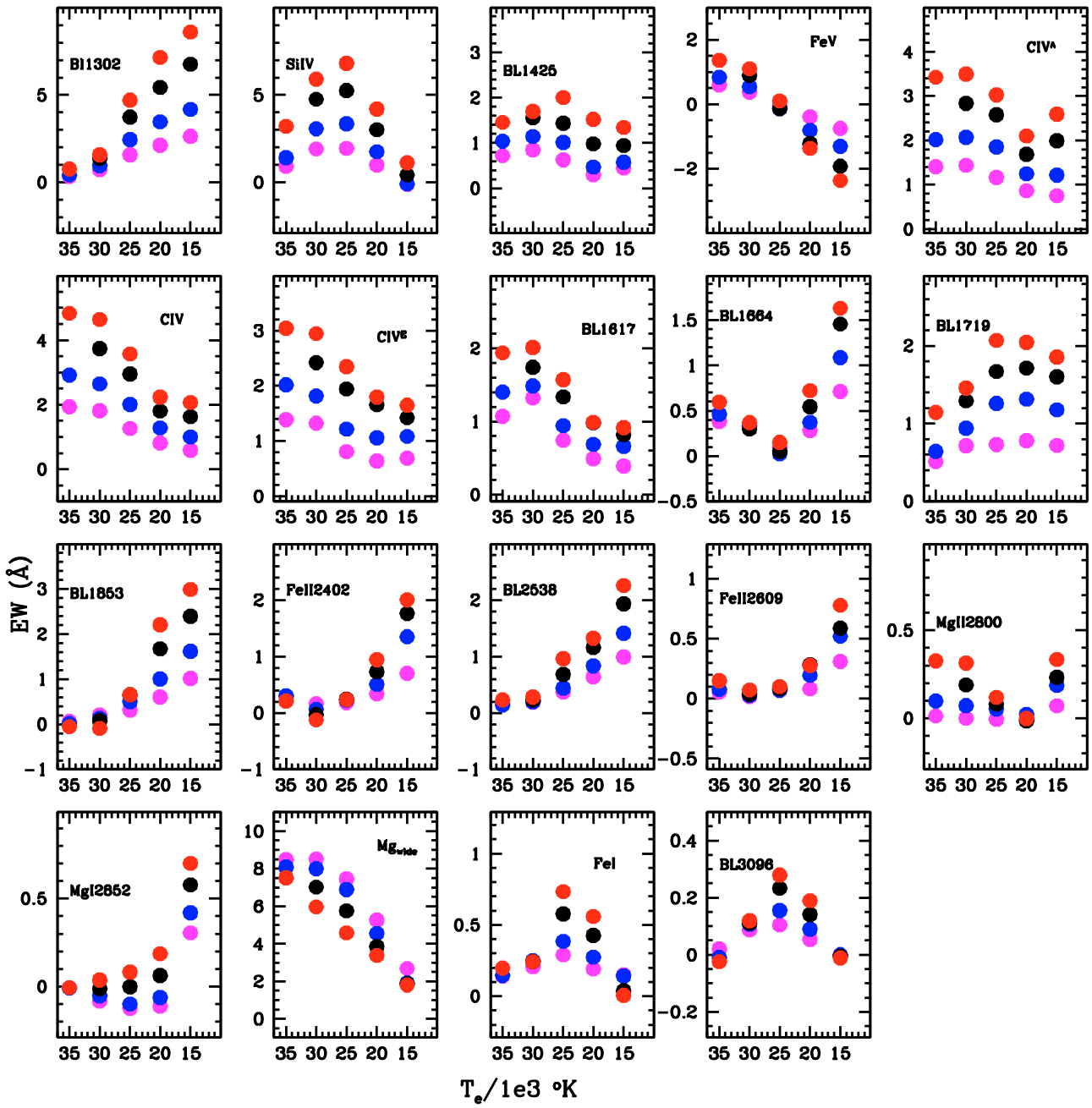

Fig. 6. Metallicity dependence of individual indices calculated on the Kurucz high-resolution synthetic spectra (smoothed to the IUE resolution of 6 Å) with gravity $\log g = 4$ and various temperatures. Colours code the metallicity, with red, black, blue and magenta displaying [Fe/H] = +0.3, 0, −0.5, −1, respectively.

Figure 6 shows the effect of metallicity on the *EW*s of individual indices, as a function of temperature, for a constant gravity of $\log g = 4$. Indices have been calculated on the high-resolution Kurucz spectra of Rodríguez-Merino et al. (2005), after smoothing the spectra to the IUE resolution. We briefly comment on the most relevant trends as a wider discussion can be found in Chavez et al. (2007), where the focus is on stellar indices, while the focus of this paper is on stellar population models.

Indices generally react to metallicity with higher metallicites (red) displaying stronger *EW*s. There are however some interesting exceptions. The mid-*UV* index BL3096 is almost insensitive to metallicity, as already pointed out by Chavez et al. (2007), which makes it in principle a potential age-indicator. The indices FeV and Mg_{wide} display stronger *EW*s at the lowest metallicities, the index FeV showing such inversion around a temperature of 25 000 K. The effect on the Mg_{wide} index is very small and confined to the very high temperatures.

Metallicity effects will be further commented on using the computed SSP models in the next section.

In order to estimate fractional metallicity corrections we consider the separate effects of abundance changes on the absorption feature and on the pseudo-continuum fluxes, which are expressed by the multiplicative factors $\alpha(T_{\rm eff})$ and $\beta(T_{\rm eff})$:

$$\begin{aligned} S_{\rm NS} &= \alpha(T_{\rm eff}) S_{\odot} \\ C_{\rm NS} &= \beta(T_{\rm eff}) C_{\odot} \end{aligned} \quad (8)$$

$\alpha(T_{\rm eff})$ and $\beta(T_{\rm eff})$ are the ratios of the non-solar and solar fluxes in the line and the continuum, respectively, and are calculated from theoretical spectra.

Taking Eq. (8) into consideration, the non-solar FF ($\phi_{\rm NS}$) is written as:

$$\phi_{\rm NS} = \left(1 - \frac{\alpha(T_{\rm eff})S_\odot}{\beta(T_{\rm eff})C_\odot}\right)\Delta\lambda, \quad (9)$$

which we can express in terms of the solar FF ($\phi_\odot$) as follows:

$$\phi_{\rm NS} = \left[1 - \frac{\alpha}{\beta}\left(1 - \frac{\phi_\odot}{\Delta\lambda}\right)\right]\Delta\lambda. \quad (10)$$

The FF calculated this way are plugged into the M05 EPS code to produce integrated indices for metallicities 2, 1/2 and 1/20 $Z_\odot$.

An alternative way to estimate the metallicity corrections consists of calculating the differential effect of abundance changes on the equivalent widths, computed again from the Kurucz theoretical spectra, and applying this differential at each temperature to the solar FF:

$$\phi_{\rm NS} = \phi_\odot + \Delta EW_{\rm K}. \quad (11)$$

In this case we would be assuming that second order metallicity effects $O(\Delta[{\rm Z/H}]^2)$ are negligible. The comparisons we ran (not shown here for space considerations) showed that both approaches yield virtually the same results.

5. Integrated line indices of stellar populations models

We calculate the integrated line indices of stellar population models by following two approaches as described in the next two subsections. Synthetic line indices are obtained for SSP, i.e. instantaneous and chemically homogeneous bursts, with ages $t \gtrsim 1$ Myr and various metallicities (2 $Z_\odot$, $Z_\odot$, 1/2 $Z_\odot$ and 1/20 $Z_\odot$), and for composite stellar populations of solar metallicity. The IMF of the models is the Salpeter (1955) one. We have checked that the values of the line indices remain almost unchanged whether we use the Kroupa (2001) or a top-heavy IMF, with exponent 1 in the notation in which the Salpeter one is 2.35.

In both cases, the model line indices are tested with globular cluster data (Sect. 6).

5.1. Empirical indices of stellar population models

We use the FFs described in Sect. 4 to assign empirically-based line indices to each star of the synthetic population. These are then added in order to obtain the integrated line index of the whole population. The integrated line index $EW_{\rm P}$ can be expressed for an SSP as the sum of the continuum-flux weighted line indices of the stars (Maraston et al. 2003):

$$EW_{\rm P} = \sum_i \beta_i EW_i. \quad (12)$$

β_i is the weighting factor, which takes into account the relative contribution of the ith star of the population to the continuum flux. The uncertainty on the integrated equivalent width follows as:

$$\sigma^2_{\rm P} = \sum_i \beta_i \sigma^2_{EW_i} \quad (13)$$

where $\sigma^2_{EW_i}$ is the uncertainty on the equivalent width of the ith star.

Since by construction the residuals of the fitting procedure are randomly distributed in the $T_{\rm eff}$ and $\log g$ space, we can assume that the uncertainty is equal to the standard error of the residuals $\sigma_{\rm res}$ defined as:

$$\sigma_{\rm res} = \sqrt{\frac{1}{N-1}\sum_j^N (R_j - \bar{R})^2} \quad (14)$$

where $R_j = EW^*_j - EW_j$ is the difference between the equivalent width predicted by the FF (EW^*_j) and the measured one (EW_j), and N is the number of stellar groups contributing to the fit. Therefore $\sigma^2_{EW_i} = {\sigma_{\rm res}}^2$ can be taken out from the sum in Eq. (13) and, since by definition $\sum_i \beta_i = 1$, we get $\sigma_{\rm P} \equiv \sigma_{\rm res}$.

5.2. Theoretical indices of stellar population models

In parallel to the FF-based approach, we calculate the integrated line indices via direct integration on the synthetic spectral energy distribution (SED) of the M05 stellar population models. We computed a version of the M05 stellar population models using as input the *UV*BLUE library by Rodríguez-Merino et al. (2005). The *UV*BLUE is based on LTE calculations carried out with the ATLAS9 and the SYNTHE codes developed by Kurucz (1979), and spectra are provided for a wide range of chemical compositions, gravities and temperatures. The wavelength range is 850–4700 Å. The spectral resolution is very high $\lambda/\Delta\lambda \sim 50\,000$. The authors compare the library with IUE spectra of stars with known atmospheric parameters and find an overall good agreement for stars of types B to G5 and for most spectral features. Exceptions are the CIV line for O, B and to a lesser extent A-type stars and the spectral region 2400 to 2700 Å in the mid-*UV* of F to G stars. In general the authors note that the discrepancy is worse in giants than in dwarfs.

In Fig. 7 we compare the *UV* indices as measured on the individual IUE observed stars and Kurucz stellar spectra, as a function of temperature for a fixed gravity ($\log g = 4$ in the Kurucz spectra and ≥3.8 for the IUE stars). The figure shows that several indices are consistent between the real and the synthetic stars, while others such as BL1302, SiIV (for some temperatures) and BL1425 are discrepant, a fact that will propagate into the stellar population models. When the indices are discrepant, the real stars often, but not always, have stronger indices. Some of these effects may originate from abundance ratio effects, others from a wrong stellar parameter assignment (as discussed by Rodríguez-Merino et al. 2005) or by incomplete line-lists in the theoretical models. For the far-*UV* indices the discrepancies may arise from non-LTE effects, stellar winds, etc. (Pauldrach et al. 2001; Dorman et al. 1993; Chavez et al. 2007).

We have computed the stellar population models using the original high-resolution *UV*BLUE library and then smoothed them using a Gaussian filter convolution in order to match the 6 Å resolution of the IUE spectra. We refer to these as Kurucz-high-resolution based M05 models.

The SED-based line indices will give us insights into how well the Kurucz spectra reproduce stellar absorptions in the *UV*. It is interesting to note that we resorted to this approach after having found for some indices severe discrepancies between the LMC GCs data and the Milky Way FF-based models.

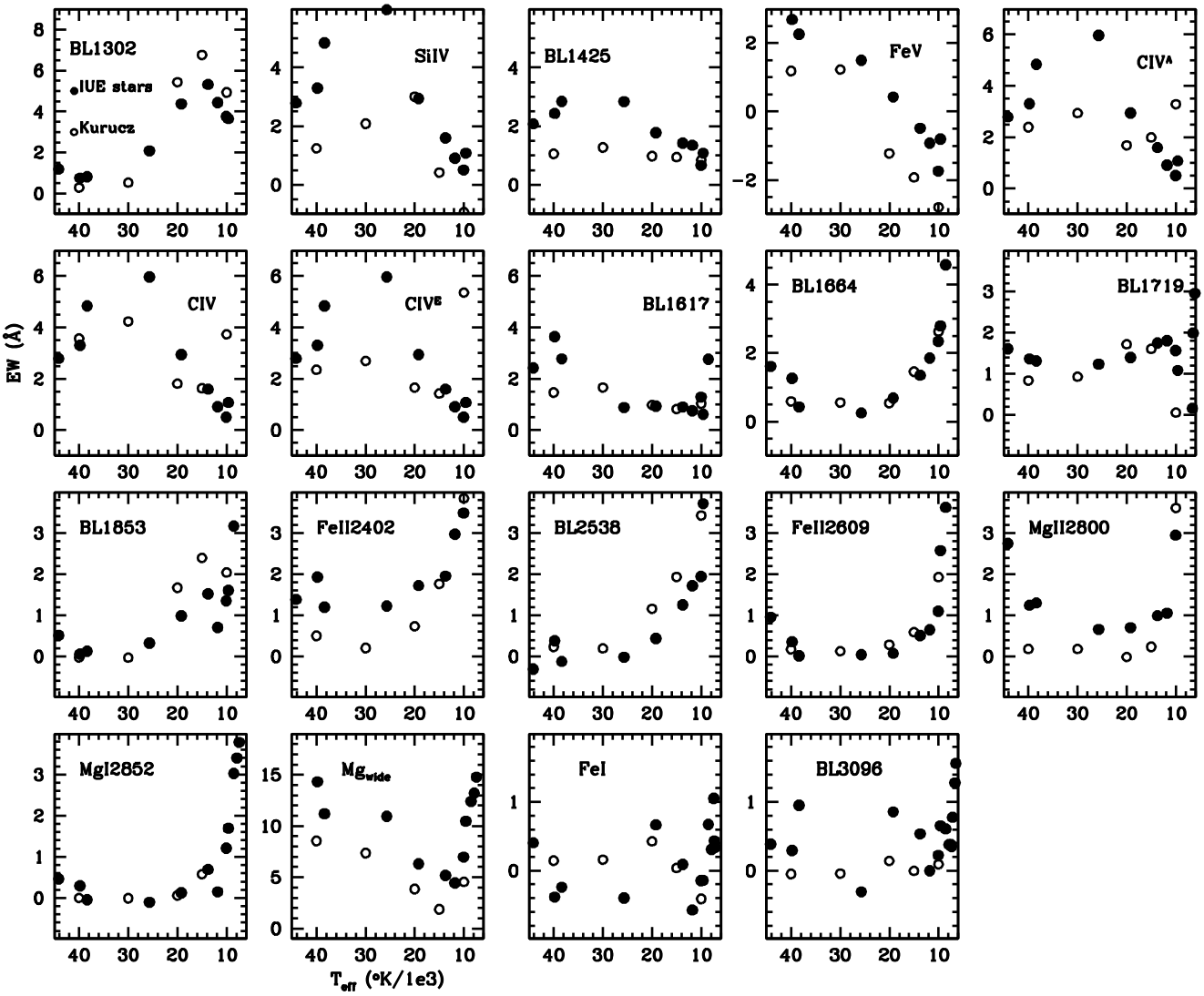

Fig. 7. Comparison between the indices of individual stars from the F92 IUE library (filled symbols) and those computed on solar metallicity Kurucz-*UV*BLUE synthetic spectra (smoothed to the IUE resolution of 6 Å) with gravity $\log g = 4$ and various temperatures (open symbols).

5.3. Age and metallicity sensitivity of individual indices

We use the models computed using the high-resolution Kurucz library to determine the age and metallicity sensitivity of the individual line indices.

Figure 8 shows the time evolution of synthetic line indices of SSP for different total metallicities (2, 1, 1/2 and 1/20 $Z_\odot$).

The dependence on age of indices is straightforward: all indices evolve strongly with age, which is due to the fast evolution of the temperature of the turnoff mass at these low ages.

Metallicity effects are sometimes more complex, as in some cases temperature effects on the continuum and the effects of the actual absorbers in the lines cancel each other and produce an insensitivity of the line indices to metallicity. In the optical region, metal line indices decrease in strength with decreasing metallicity, and vice versa. In the *UV*, the behaviour of the integrated indices depends more strongly on the turnoff temperature, whose effect can dominate over the abundance effect on the line itself (see also discussion in Chavez et al. 2007). At a given temperature, lower metallicity stars tend to display weaker absorption lines due to lower opacity. At a given age, on the other hand, stars around the MSTO become hotter as metallicity decreases, which may strengthen the lines in some indices and temperature ranges (remember that MSTO stars are the main contributors to the integrated indices), thereby balancing the pure abundance effect. Which effect dominates depends on the index and on the temperature range (and therefore on the age of the SSP). In general far-*UV* indices show higher equivalent widths for higher temperatures, while mid-*UV* indices display the opposite behaviour.

In general, lower *EW*s correspond to sub-solar chemical compositions, but the temperature dependence is complex. The line indices C IV, C^A_{IV} and BL_{2538} behave regularly along the whole range of temperatures calculated, while the Si IV and BL_{1425} lines do so until $T_{\rm eff} \sim 15$ kK (mid B spectral type), while at lower temperatures metallicity effects vanish. The line BL_{1617} is attributed to transitions of Fe IV and Fe V (Dean & Bruhweiler 1985) however it shows little variation with the total chemical composition. We have confirmed this trend (for $T_{\rm eff} > 20$ kK), by computing synthetic spectra models with the WM-basic software (Pauldrach et al. 2001) for solar and half-solar metallicity. The difference ΔEW was found to be less than 0.2 Å and comparable with the results obtained with the Kurucz spectra. The line BL_{1664} behaves similarly to BL_{1617}, but is very strong at

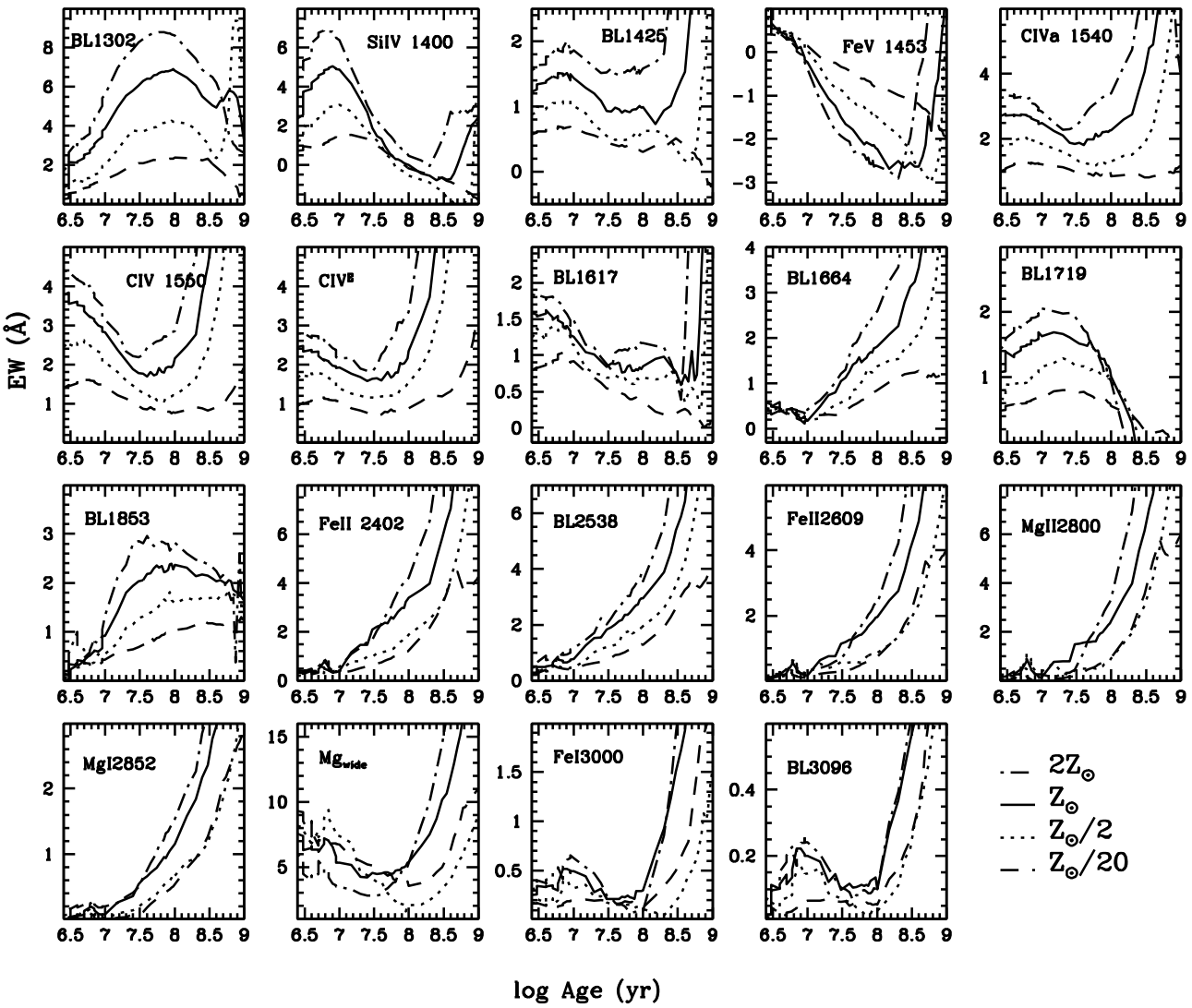

Fig. 8. Effect of age and metallicity on line indices of SSP models.

high metallicity. Most likely for these two lines the effect of increasing metallicity mainly works in depressing the continuum, which has the effect of lowering the line-strength.

Si IV and C IV indices display the strongest sensitivity to metallicity at ages below 50 Myr, while BL_{1853} is a good metallicity indicator at older ages. BL_{1617} and FeV show a remarkable insensitivity to metallicity at young ages. Though only up to ages around 60 Myr and 20 Myr respectively, these lines are potentially powerful age indicators. FeV is the only index that becomes stronger in lower metallicity populations at ages larger then 20 Myr.

6. Testing the indices with real data

6.1. Globular cluster templates

Before using the models to study complicated stellar populations like galaxies, it is necessary to test them on globular clusters (GCs) with independently known ages, metallicities and abundance ratios (e.g., Renzini & Fusi Pecci 1988; Worthey 1994b; Maraston et al. 2003; Leonardi & Rose 2003; Beasley et al. 2002; Proctor et al. 2004; Lee & Worthey 2005; Schiavon 2007; Koleva et al. 2008; Graves & Schiavon 2008). GCs are the ideal templates since they are prototypical simple stellar populations.

We use *IUE* observations (Cassatella et al. 1987) of 10 GCs in the Large Magellanic Cloud (LMC), which have independent age and metallicity determinations (Table 3). Ages and metallicities were obtained from different sources. Both metallicity and the age of NGC 1711 were taken from Dirsch et al. (2000), the former was determined by using metallicity to Strömgrem colour empirical calibrations, the latter by fitting CMD to Geneva (Schaerer et al. 1993) and Padova (Bertelli et al. 1994) isochrones. Age estimates for NGC 1805 and NGC 1818 were taken from the review by de Grijs et al. (2002) and metallicities from Johnson et al. (2001) (who used fits to near-infrared HST CMDs). Ages for all the other clusters come from Elson (1991) and Elson & Fall (1988) and were estimated using optical CMDs, while metallicities were estimated by matching stellar spectral models to medium resolution optical spectroscopy of individual stars for NGC 1850, NGC 1866, NGC 2004 and NGC 2100 (Jasniewicz & Thevenin 1994); infrared spectroscopy through equivalent width measurements of the 1.62 μm near-IR feature for NGC 1984 and NGC 2011 (Oliva & Origlia 1998); and from optical HST CMDs for NGC 2164 (Mackey & Gilmore 2003).

On the GC spectra, we measure the line indices listed in Table 1. These values are given in Tables B.1 and B.2 in

Table 3. Ages, metallicities and colour excess $E(B-V)$ of the sample clusters.

Name	log(age) (yr)	[Z/H]	$E(B-V)$[10]
NGC 1711	7.70 ± 0.05[1]	-0.57 ± 0.17[1]	0.14
NGC 1805	7.00 ± 0.05[2]	$-0.40 \lesssim$ [Z/H] $\lesssim 0.0$[2,5]	0.10
NGC 1818	7.40 ± 0.30[2]	$-0.40 \lesssim$ [Z/H] $\lesssim 0.0$[2,5]	0.07
NGC 1847	7.42 ± 0.30[4]	-0.37[9]	0.09
NGC 1850	7.40 ± 0.20[3]	-0.12 ± 0.20[6]	0.09
NGC 1866	8.12 ± 0.30[4]	-0.50 ± 0.10[6]	0.07
NGC 1984	7.06 ± 0.30[4]	-0.90 ± 0.40[8]	0.14
NGC 2004	7.30 ± 0.20[3]	-0.56 ± 0.20[6]	0.09
NGC 2011	6.99 ± 0.30[4]	-0.47 ± 0.40[8]	0.08[11]
NGC 2100	7.20 ± 0.20[3]	-0.32 ± 0.20[6]	0.19

References: [1] Dirsch et al. (2000); [2] de Grijs et al. (2002); [3] Elson (1991);[4] Elson & Fall (1988); [5] Johnson et al. (2001); [6] Jasniewicz & Thevenin (1994); [7] Hill et al. (2000); [8] Oliva & Origlia (1998); [9] Mackey & Gilmore (2003); [10] colour excess from: Cassatella et al. (1987), with the exception of NGC 2011; [11] Persson et al. (1983). For NGC 1847 no error on metallicity is given and we have conservatively assumed 0.2, a value common to most globular clusters.

Appendix A together with estimates of the associated errors. The uncertainties of the measured equivalent widths are calculated in the same way as we estimated the errors for the measurements on the stellar group spectra (see Sect. 3.2), but using the error spectra provided directly by the IUE observations. Since the maximum age of the template GCs is 130 Myr and mid-*UV* indices are significantly strong only for populations older than this limit, we are not able to check most of the synthetic mid-*UV* line indices. This would be possible in the future, provided that good quality observations of older clusters are carried out in the *UV*.

6.2. Far-UV indices

Figure 9 shows the comparison of SSP synthetic line indices in the far-*UV* with GCs data. For three metallicities, solar, half-solar and Z 1/20 $Z_{\odot}$, two sets of models are shown, those based on the empirical-IUE FFs (solid lines) and those on the M05 SEDs using as input the high-resolution Kurucz-based synthetic stellar library (dashed lines).

Strictly speaking, due to the sub-solar metallicity of the LMC star clusters, only sub-solar models can be meaningfully checked with these data. However, since the solar-metallicity models are those uniquely locked to the IUE-based FFs and are not dependent on our recipe for inserting metallicity effects, we plot them as well. When we calculate the metallicity and the age of the LMC clusters explicitly from the indices we use the full grid of models (see Sect. 6.4).

Looking at Fig. 9 we see that theoretical and empirical models agree reasonably well and reproduce GCs data for most indices. These results, especially for C IV, are remarkable, since these line indices have been discussed as being poorly determined due to blending with interstellar lines, dust effects, and IMF effects (see discussion in Rix et al. 2004). Also Rodríguez-Merino et al. (2005) quote the C IV line as one of the most poorly described by the *UV*BLUE library.

Exceptions are BL1425 and FeV 1453 for which the empirical models lie above the data.

Errors in the fitting functions can be excluded, since the same discrepancy is found in the stellar population models of Bruzual & Charlot (2003) that use as input spectral library the F92 without passing through the fitting function procedure (see Sect. 6.5, Fig. 16).

Abundance effects, for example an under abundance of iron in the LMC GCs as compared to the IUE MW stars, also seem unlikely as neither the solar-scaled Kurucz-based models nor the Starburst99 models based on a higher-resolution version of the IUE library show the same discrepancy (see Sect. 6.5). In addition, other iron-sensitive line-indices like Bl1617 do not behave the same way. For the same reasons an iron enhancement in the IUE stars can also be ruled out.

An effect from interstellar lines appears unlikely for several reasons. Interstellar lines exist at these wavelengths (see e.g. Castelli et al. 1984) but they are known also to affect the SiIV and CIV indices (Castelli et al. 1984; Robert et al. 1993) whereas such a sizable discrepancy is not evident for the other indices in Fig. 9. In addition, the Starburst99 models do not show the same discrepancy and they have also not been corrected for interstellar lines (Robert et al. 1993). Also it could be argued that interstellar lines affect the GCs in a similar way as the empirical models that are constructed using real stars, and if at all it should be Kurucz-based models that are discrepant, as theoretical spectra do not incorporate the effect of interstellar lines.

Finally, note that in case of BL1302 and BL1853 the empirical models would fit the data for metallicities above solar, which is too high. We come back to this point later when we use the indices to derive quantitatively metallicities and ages.

6.3. mid-UV indices

Figure 10 is the analogue of Fig. 9 for indices in the mid-*UV* ($\lambda > 2000$ Å).

The validation of the mid-*UV* indices is less conclusive since the ages of the Cassatella et al. GCs are limited to 130 Myr, while older ages are required to set constraints on this spectral region.

In spite of the age limitation, glancing at Fig. 10 one sees that most synthetic indices are discrepant to those measured in the GCs, the FeII2402 and the Mg_{wide} being perhaps the only indices for which, given the large error bars and scatter, one could argue that the models are not clearly offset.

The reasons for these discrepancies could be either on the model side or on the GC data side. From the GC data side one cannot exclude problems in the observed spectra in the mid-*UV*.

From the model point of view, problems with the FF approach can be excluded as the comparison with the BC03 models confirms the discrepancies (Fig. 16).

One could argue that element abundance ratio effects start affecting the indices in the mid-*UV* as we know they affect most optical indices. For example an overabundance of Magnesium in the LMC GCs may push the data off the models. On the other hand, the iron lines are sometimes above and sometimes below the models and no clear pattern is detectable. Clearly a modelling of abundance ratio effects in individual lines is required here, which is the scope of a future investigation.

Finally, contamination by interstellar lines that are known to affect the region of the Mg absorption at 2800 Å (Morton 1975; Castelli et al. 1984) remain the most likely possibility (see below).

For this work we have carefully checked the case of the MgII line at 2800 Å, which we discuss below as an example of a discrepant index. We choose this index as it is often used in studies of high-redshift galaxies and the adjacent spectral region is employed to measure spectroscopic redshifts for high-z galaxies (Daddi et al. 2005).

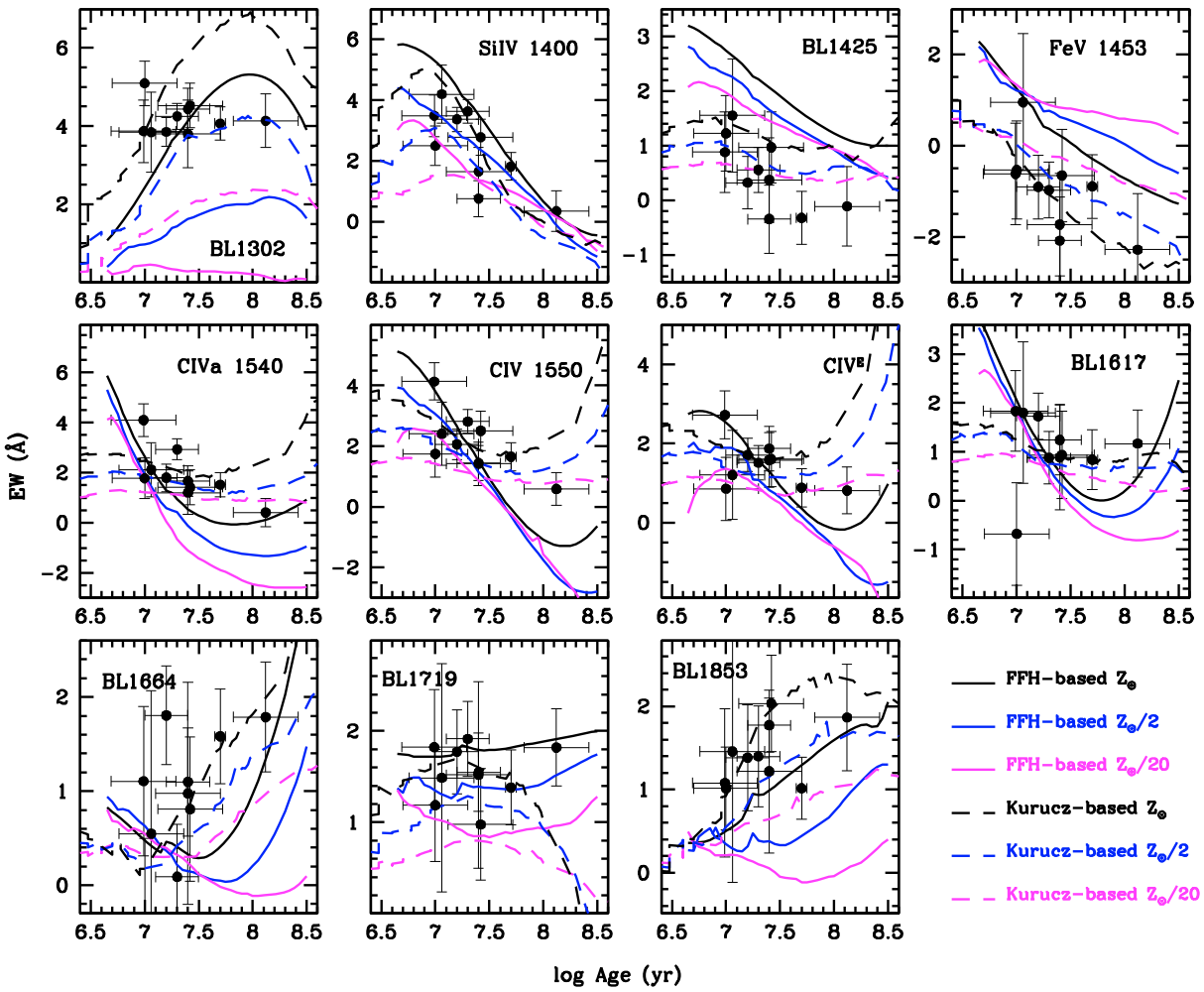

Fig. 9. Time evolution of synthetic far-*UV* line indices of simple stellar population (SSP) models, overlaid on data of LMC GCs with ages taken from the literature (symbols with error bars). Solid lines are models based on the IUE-FF while dashed lines are models based on high-resolution Kurucz model atmospheres. Black and blue lines refer to solar and half-solar metallicity, the magenta lines to Z 1/20 $Z_{\odot}$.

As we see in Fig. 10, both the empirical models and the Kurucz-based ones display significantly lower equivalent widths than the GCs. The same is true when we calculate the index on the BC03 models incorporating the F92 library direclty (dotted line in Fig. 12, upper panel). The mismatch is somewhat reduced, instead, when we apply broadband indices, such as the Mg$_{UV}$ defined by Daddi et al. (2005)[1], or the Mg$_{\rm wide}$ (see Fig. 10).

In order to understand the discrepancy we have compared the individual cluster spectra to the BC03 templates that include the Fanelli et al. library (see Fig. 11). As it can be seen the GC spectra display a much stronger magnesium absorption than the templates based on the MW stars. This explains the discrepancy seen in Fig. 12. The fact that the MgUV appears to be in better agreement with the data outlines that these indices do not trace the absorption feature but the continuum shape around those wavelength. The MgUV cannot be used to measure the magnesium abundance.

Fanelli et al. (1990; 1992) find that the Mg II (2800 Å) is very sensitive to temperature and is stronger in metal-poor stars than metal-rich ones at given effective temperature (see e.g. their Fig. 6-o), a behaviour attributed to a combination of effects, including chromospheric emission.

The case here is more complicated as the net effect is due to a stellar population and not to a single star. The clusters of our sample span a range in metallicity and some have the same age, hence the most-metal poor ones typically should have higher temperatures. However if one compares the Mg II (2800 Å) indices of these clusters (see Fig. 13), there is no indication that the most metal-poor have stronger indices.

A true abundance effect, with the LMC clusters being enriched in magnesium with respect to the MW stars of which the Fanelli et al. library is composed, finds support from the work of Beasley et al. (2002), which reports an indication of a possible magnesium overabundance in other LMC clusters of similar age from the analysis of Lick indices. The caveat we have with this interpretation is that if an abundance effect is responsible for the deep line present in the GC spectra, the overabundance of magnesium would need to be very large. In a future work we intend to study the abundance effect on the MgII2800 index as this is a potentially very powerful chemical abundance indicator for high redshift galaxies (Heap et al. 1998; McCarthy et al. 2004).

Contamination by interstellar lines originating from the warm neutral interstellar medium of the LMC (Welty et al. 1999) remains the most likely reason for the strong absorptions around the Mg region. It is interesting that the IUE stars do not show

[1] $\mathrm{Mg}_{UV} = \frac{2\int_{2625}^{2725} f_\lambda \mathrm{d}\lambda}{\int_{2525}^{2625} f_\lambda \mathrm{d}\lambda + \int_{2725}^{2825} f_\lambda \mathrm{d}\lambda}$.

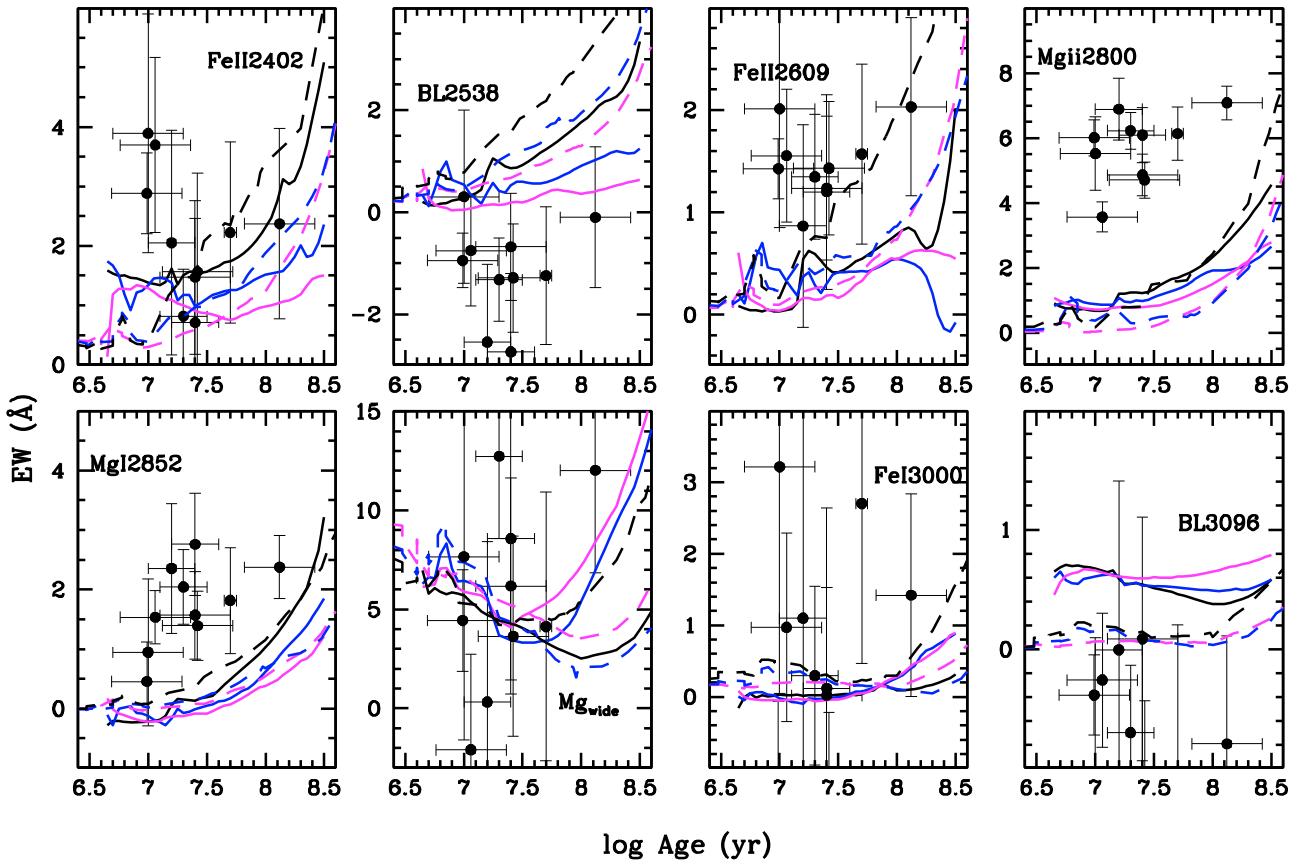

Fig. 10. Same as Fig. 9 for mid-*UV* indices.

such contamination, which may be due to the much lower extinction of galactic sitelines.

6.4. Using the indices to derive age and metallicity

Here we derive quantitatively the ages and the metallicities of the LMC clusters using the indices and compare them to the values we compiled from the literature.

For this exercise we use all eleven far-*UV* indices in case of the Kurucz-based models and seven indices, i.e. the far-*UV* indices minus BL1302, BL1425, FeV, BL1853 in case of the FF-based models. The latter choice is motivated by the clear discrepancy between the GC data and the empirical models for those indices, as we have discussed previously (see Fig. 9). Mid-*UV* indices are not considered as the agreement between models and data is generally poor. Also, the template GCs are very young and the use of the far-*UV* is more appropriate.

Ages and metallicities are derived by minimizing the quadratic distance between the measured *EW*s and the SSP models for the selected set of indices simultaneously.

The ages and metallicities we derive for the GCs from the indices are compared with literature values in Figs. 14 and 15 (values are given in Table C.1 in the Appendix).

The ages we derive from the indices are in good agreement with those compiled from the literature. This is the case for both sets of models.

The metallicities are also in satisfactory agreement considering that the metallicity dependence of the *UV* spectrum is not as straightforward as in the optical (see also discussion in Chavez et al. 2007) and that the metallicity determinations for the GCs are not homogeneous. Here the models behave differently. The

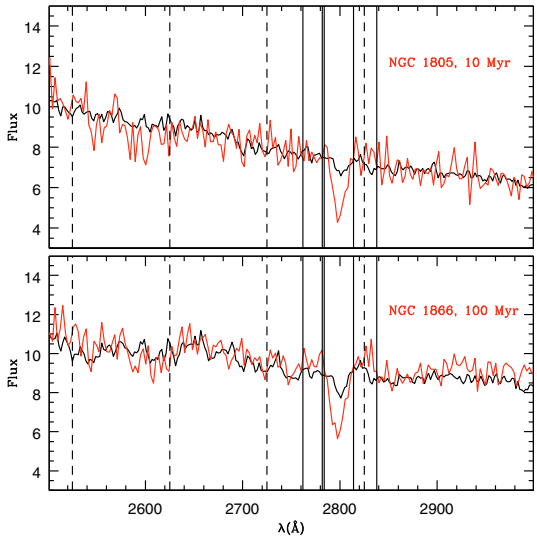

Fig. 11. Zoom of the spectral region containing the Mg II 2800 index. The observed spectra of two LMC clusters from the Cassatella et al. sample are shown in red, with overlaid template spectra from BC03 based on the Fanelli et al. library (black) at the age of the observed clusters (labeled in the panels). Vertical solid lines show the line and continua windows defining the Mg II 2800 index (cf. Table 1); dashed lines refer to the Mg$_{UV}$ of Daddi et al. (2005).

Kurucz-based models give a very good determination for more than half the sample with a tendency to lie above the literature values for three objects. The empirical models display a larger scatter, but no systematic trend. For the empirical models we

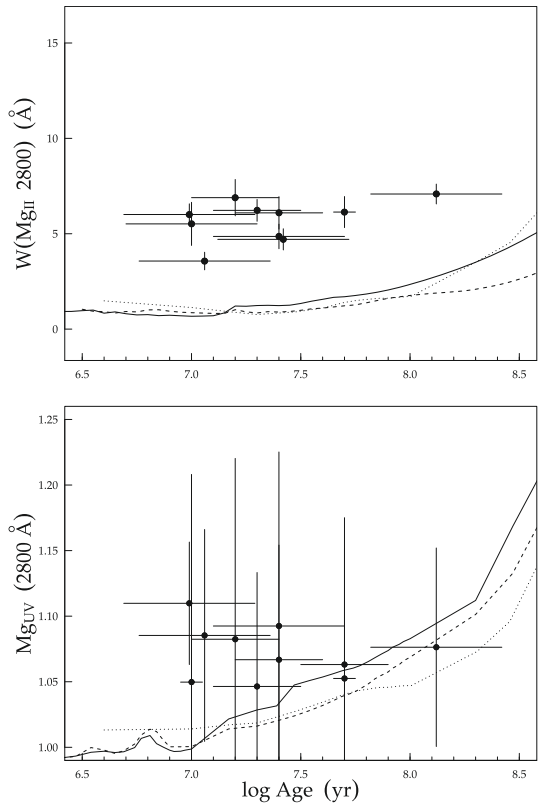

Fig. 12. Comparison between the Mg II 2800 from Fanelli et al. and the Mg$_{UV}$ index defined in Daddi et al. (2005). In both panels, solar and half-solar metallicity models (solid and dashed lines, respectively) are plotted together with the GCs data. Also plotted are the indices as derived from Bruzual & Charlot (2003) solar metallicity models (dotted line), which use the same spectral library we use in the *UV* and give very similar results to ours.

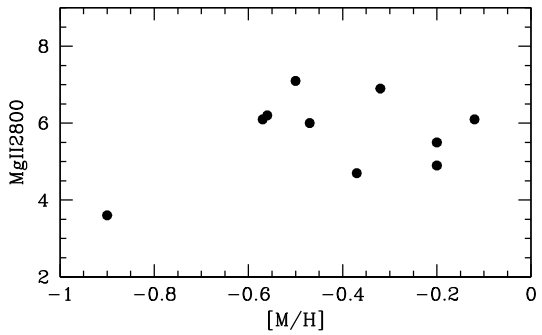

Fig. 13. The Mg II 2800 index of the LMC GCs as function of the metallicity as determined in the literature (see Table D.1 in the Appendix).

checked that had we also used the BL1302 and BL1853 indices we would have obtained systematically higher metallicities, for the reasons discussed in Sect. 6.2. When we include the two indices BL1425 and FeV for which the models are above the data, this systematic effect is rectified because the discrepancy pushes the fit to lower metallicities.

In conclusion we recommend the use of seven indices, namely SiIV, CIV^{A}, CIV, CIV^{E}, BL1617, BL1664 and BL1719, in the case of empirical models and eleven indices namely BL1302, SiIV, BL1425, FeV, CIV^{A}, CIV, CIV^{E}, BL1617, BL1664, BL1719, BL1853 for the Kurucz-based models.

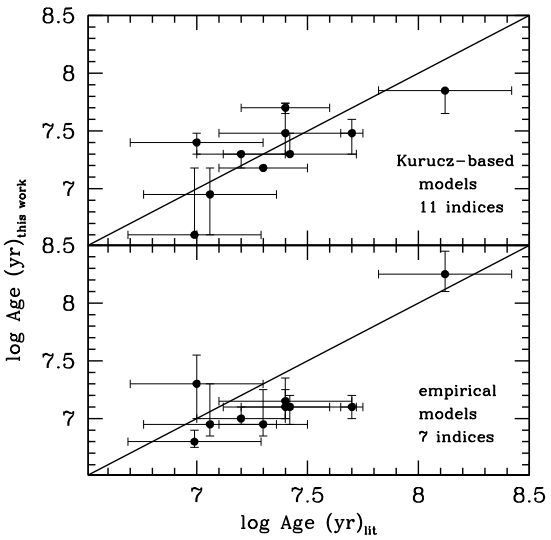

Fig. 14. Age estimates derived from all 11 far-*UV* indices for the Kurucz-based models (*upper panel*) and from seven indices for the empirical models compared to the literature values.

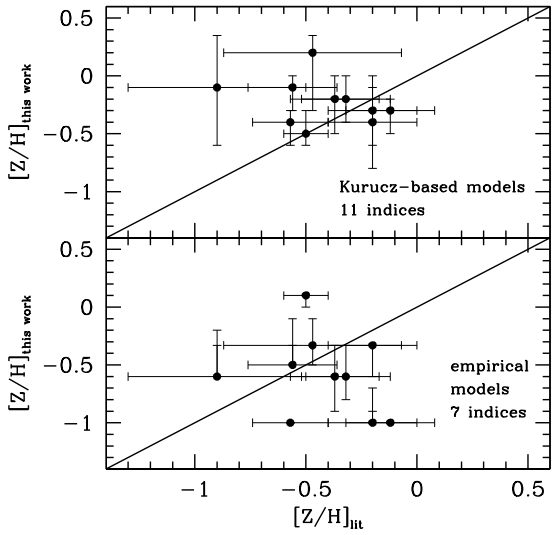

Fig. 15. Same as in Fig. 14 for metallicity.

It will be interesting to apply this age and metallicity tool to distant galaxies for which many rest-frame *UV* spectra are available in the literature.

6.5. Models based on other tracks or spectral libraries

No other model in the literature provides all the line indices we present here. Still, we can use the integrated spectral energy distributions of other population synthesis models and obtain the line-indices by direct integration. Two models are interesting in this context, the Bruzual & Charlot (2003) and *Starburst 99* (Leitherer et al. 1999) models. The reason is that the former adopt the Padova tracks and the same spectral library we use (F92). This allows us to check the joint effect of stellar tracks and our fitting function procedure. Though we cannot separate the two effects, we should be able to use this comparison to detect gross discrepancies due to the fitting function procedure. On the other hand, *Starburst 99* uses the same stellar tracks as in the M05 models, but a different spectral library (described in Robert et al. 1993), mostly based on high-resolution *IUE* spectra from

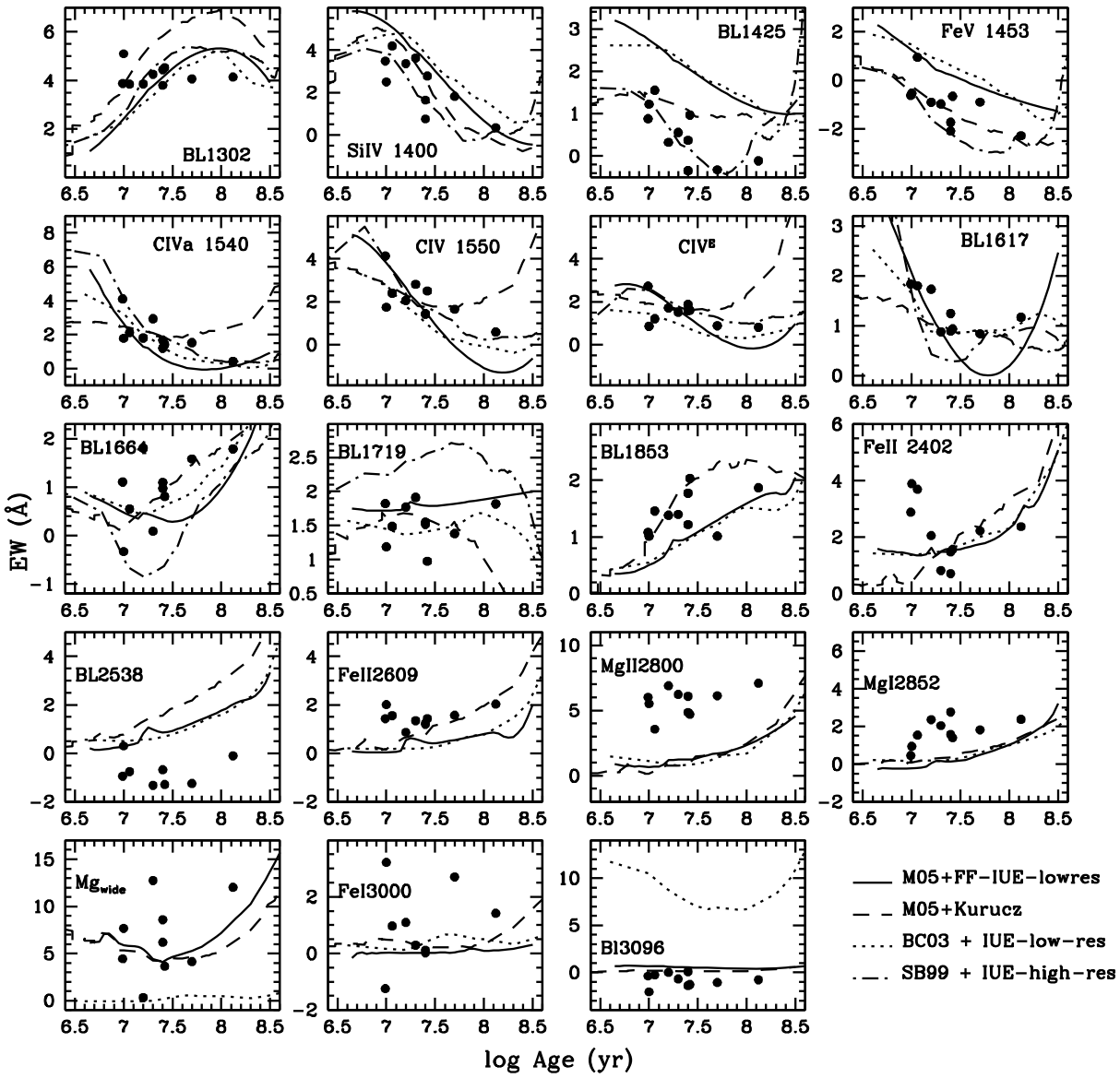

Fig. 16. Comparison between several model indices at solar metallicity. Our FF-based (solid) and Kurucz-based (dashed) indices are compared to those we calculate on the Bruzual & Charlot (2003) (dotted) and Leitherer et al. (1999) (dashed-dotted) models. Bruzual & Charlot (2003) use F92 spectral library and Leitherer et al. (1999) use a higher-dispersion version of *IUE* spectra in addition to the F92 library (Robert et al. 1993).

Howarth & Prinja (1989). Hence with the *Starburst 99* models we can check the effect of the spectral library[2].

Figure 16 shows the results of our comparison. In general, the indices behave similarly in most cases, suggesting that our conclusions are robust against different stellar tracks and different empirical libraries.

The discrepancies between the FF-based models of the indices BL_{1425} and FeV 1453 and the template GCs is found also when the Bruzual & Charlot (2003) SEDs are used (dotted line). This excludes that the origin of the discrepancies lies in an error of the FF approach. The fact that the *Starburst 99*-based indices do not display the same discrepancy suggests that the origin of the mismatch lies in the O-star IUE-low-resolution library.

All the discrepant indices in the mid-*UV* remain discrepant also for the BC03 models in which the F92 library is used without passing through FF, again excluding a major problem in the FF procedure.

6.6. The effect of mass-loss

Very massive stars are known to suffer from strong mass-loss, a process driven essentially by radiation pressure which is very difficult to predict by stellar evolution models. For this reason we have investigated the effect, if any, of varying the recipes used in the stellar tracks for the mass-loss rates on the upper part of the IMF. We computed solar metallicity models, using as inputs isochrones from the Geneva group (Meynet et al. 1994), which implement a higher mass-loss rates (twice the one used in their standard tracks) for the very massive stars ($\gtrsim$15 $M_\odot$).

We show in Fig. 17 the case of the Si IV 1400 absorption index, as an illustration of the general case. The doubling of the mass-loss rate has a negligible effect on the indices.

[2] To allow for a meaningful comparison, we have smoothed the SEDs of *Starburst 99* to the same resolution as the F92 library (6 Å).

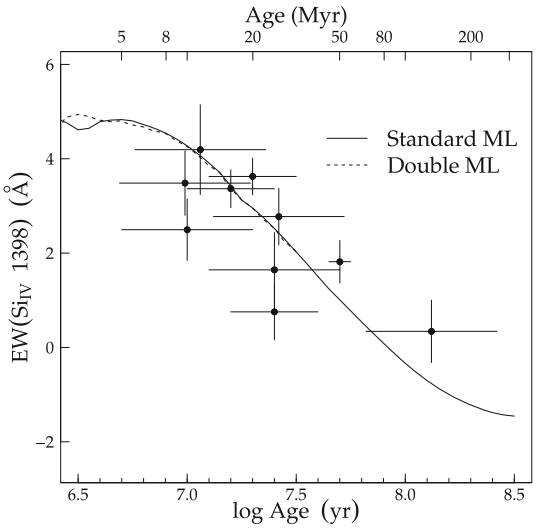

Fig. 17. Comparison between models adopting Geneva tracks with a standard (solid line) and twice the standard (dashed line) mass-loss rate for massive stars ($\gtrsim$15 $M_{\odot}$). No effect is appreciable.

7. Summary and conclusions

We have exploited the low-resolution (6 Å) absorption line index system in the far and mid-*UV* as defined by Fanelli et al. (1992) based on the IUE low-resolution stellar library. Though the latter work was published sixteen years ago, it remains the most comprehensive study of *UV* stellar absorption lines that is based on real stars. Surprisingly, it has not yet been used for population synthesis studies. Our aim is to construct integrated line-indices of stellar population models that can be used as age and metallicity indicators of young stellar populations in the local Universe or at high redshift. In total we model 19 indices in the wavelength range ~1200 Å to ~3000 Å.

We follow a two-fold strategy. First, we have constructed analytical approximations (fitting functions) to the empirical line indices measured in single stars, as functions of the stellar parameters gravity and temperature. This approach has been used as the FFs can be conveniently inserted in population synthesis models and because fluctuations in the spectra of stars with similar atmospheric parameters are averaged out[3]. The IUE empirical library contains mostly stars with solar metallicity. We then inserted a metallicity dependence in the fitting functions by means of Kurucz synthetic spectra. As a next step, the fitting functions were plugged into an evolutionary synthesis code in order to compute integrated line indices of stellar population models as a function of the age and metallicity of the stellar population. In this way we have calculated semi-empirical model indices of stellar populations.

In parallel we have used a high-resolution version of the Kurucz theoretical spectral library (Rodriguez-Merinos et al. 2005) to construct high-resolution SEDs of the M05 stellar population models and computed the *UV* indices directly on these SEDs. This gives us theoretical model indices of stellar populations[4].

We have checked both models by comparing the synthetic line-indices with IUE data of template globular clusters in the Magellanic Clouds with independently known ages – from 10 Myr to 0.13 Gyr – and metallicities.

[3] The fitting functions are given in the appendix.

[4] Both types of model indices as well as the high-resolution model SEDs are available at `http://www.maraston.eu`

Most of the far-*UV* indices are found to be in satisfactory agreement with the models. The lines of C IV and Si IV already have been studied extensively in the literature (Storchi-Bergmann et al. 1994; Leitherer & Heckman 1995; Leitherer et al. 1999; Heckman et al. 1998; Rix et al. 2004). We add here their validation with GCs. The other indices instead are modelled and compared with globular clusters in this work for the first time.

The models of most mid-*UV* indices, instead, fail to reproduce the GC data. Given that the GC are young (<0.13 Gyr) and mid-*UV* indices are strong in older populations, one cannot rule out a problem in the mid-*UV* part of the GC observed spectra. We shall pursue this aspect in a future paper.

For a quantitative test we have calculated the ages and metallicities we derive for the GCs using both empirical and Kurucz-based models. For the empirical models we use seven indices (SiIV, CIV^{A}, CIV, CIV^{E}, BL1617, BL1664, BL1719) whereas for the Kurucz-based models we could use all eleven indices in the far-*UV* (see Fig. 9).

For these selected sets of indices we find good agreement between the ages and metallicities we derived based on the indices and the values given in the literature. These sets can now be applied to age and metallicity derivations for distant galaxies.

It is important to note that the theoretical models presented here refer to solar-scaled abundance ratios of chemical elements, while the empirical models refer to the pattern of the Milky Way stars out of which the input library is constructed. On the other hand, some evidence has been reported in the literature of enhancement of α-elements with respect to iron in Magellanic Cloud globular clusters (Oliva & Origlia 1998; Beasley et al. 2002). Given the satisfactory agreement we obtain in the derived ages and metallicities of the LMC GCs one tends to conclude that, at least when using our selected set of far-*UV* indices, possible chemical abundance anomalies do not matter. Nonetheless, we are following up the modelling of *UV* indices for various abundance ratios that will hopefully clarify this issue.

Acknowledgements. We are grateful to the anonymous referee for prompt replies and constructive comments that significantly improved the paper, and to Christy Tremonti and Guinevere Kauffmann for clarifying comments. C.M. and D.T. acknowledge the ospitality of the European Southern Observatory Visitor Programme during which this work was completed. C.M. is a Marie Curie Excellence Grant Team Leader and ackwnoledges grant MEXT-CT-2006-042754 of the European Community.

Appendix A: Coefficients of the fitting functions

Here we provide the numerical coefficients of the FFs and the ranges in temperature and gravity inside which the fitting functions are valid (Table A.1). The fitting functions should not be extrapolated outside these regions. The equivalent width at all temperatures and surface gravities inside the validity range is the third degree polynomial given by the coefficients listed in Table A.1 and Eq. (5) in Sect. 4. When a two-region fit is necessary to construct the FF, each local FF (cool and hot) has to be applied in its corresponding region. Equation (6) applies in the overlapping region.

Appendix B: Absorption line-indices of LMC globular clusters

In Tables B.1 and B.2 we list our measurements of the *UV* absorption line-indices in the LMC globular cluster spectra.

Table A.1. Coefficients of the empirical fitting functions. Some indices required fits performed in adjacent temperature regions (see Sect. 4), in such cases the first row refers to the cool region and the second one to the hot. The continuity between the two functions is obtained using a cosin function (see Eq. (6)). Validity limits in $\log g$ and $\log T_{\rm eff}$ are defined by the coolest and hottest stellar groups, and the maximum and minimum values of surface gravity available in the library that was included in the fit. These are: $\log T_{\rm eff} = 4.67-3.86$ and $\log g = 1.4-4.1$ for far-*UV* indices, and $\log T_{\rm eff} = 4.67-3.78$ and $\log g = 1.2-4.3$ for mid-*UV* indices.

Index	a_0	$\log T_{\rm eff}$	$\log g$	$\log T_{\rm eff}^2$	$\log T_{\rm eff} \log g$	$\log g^2$	$\log T_{\rm eff}^3$	$\log T_{\rm eff}^2 \log g$	$\log T_{\rm eff} \log g^2$	$\log g^3$
BL_{1302}	–7.410092e+03	5.161229e+03	–2.104500e+01	–1.190241e+03	5.089514e+00	0.000000e+00	9.087288e+01	0.000000e+00	0.000000e+00	0.000000e+00
Si IV	8.329603e+03	–5.950179e+03	0.000000e+00	1.413073e+03	0.000000e+00	0.000000e+00	–1.114978e+02	0.000000e+00	0.000000e+00	–4.464140e-02
BL_{1425}	2.801138e+03	–1.887279e+03	–1.124998e+02	4.198010e+02	5.522990e+01	0.000000e+00	–3.073181e+01	–6.792400e+00	0.000000e+00	0.000000e+00
Fe V	0.000000e+00	0.000000e+00	0.000000e+00	–5.370300e+00	4.218601e+00	0.000000e+00	1.291487e+00	–1.022240e+00	0.000000e+00	0.000000e+00
C_{IV}^A	0.000000e+00	9.475584e+01	0.000000e+00	–5.981724e+01	1.591892e+01	0.000000e+0.0	9.063165e+00	–3.998758e+00	0.000000e+00	0.000000e+00
C IV	1.160656e+04	–8.160319e+03	0.000000e+00	1.908096e+03	0.000000e+00	0.000000e+00	–1.483084e+02	0.000000e+00	–6.465476e-02	0.000000e+00
C_{IV}^E	1.146391e+04	–8.060925e+03	0.000000e+00	1.886312e+03	0.000000e+00	0.000000e+00	–1.468829e+02	0.000000e+00	0.000000e+00	0.000000e+00
BL_{1617}	7.195609e+03	–4.969059e+03	1.637501e+01	1.134789e+03	0.000000e+00	0.000000e+00	–8.554261e+01	–1.010919e+00	0.000000e+00	0.000000e+00
BL_{1664}	3.99173e+03	–2.69840e+03	0.000000e+00	6.070700e+02	0.000000e+00	0.000000e+00	–4.545000e+01	0.000000e+00	0.000000e+00	0.000000e+00
BL_{1719}	0.000000e+00	0.946425e+00	1.39515e+00	0.000000e+00	–0.463588e+00	0.000000e+00	0.000000e+00	0.000000e+00	0.000000e+00	0.000000e+00
BL_{1853}	–3.992238e+04	3.132500e+04	–8.032732e+02	–8.174011e+03	4.072430e+02	0.000000e+00	7.093685e+02	–5.124554e+01	–2.300320e-01	0.000000e+00
	–1.741241e+03	1.236778e+03	0.000000e+00	–2.912705e+02	–1.240263e-01	0.000000e+00	2.278486e+01	0.000000e+00	0.000000e+00	0.000000e+00
Fe II 2402	–1.025711e+05	7.846243e+04	0.000000e+00	–1.997183e+04	–1.152896e+01	0.000000e+00	1.691469e+03	3.738713e+00	–5.328224e-01	0.000000e+00
	4.187948e+03	–2.837521e+03	0.000000e+00	6.404977e+02	0.000000e+00	0.000000e+00	–4.814913e+01	0.000000e+00	0.000000e+00	0.000000e+00
BL_{2538}	–5.765329e+04	4.594702e+04	–1.525047e+03	–1.220363e+04	8.150653e+02	0.000000e+00	1.080533e+03	–1.101304e+02	2.225463e+00	–9.983048e-01
	2.215483e+02	–9.798301e+01	0.000000e+00	1.083353e+01	0.000000e+00	0.000000e+00	0.000000e+00	0.000000e+00	0.000000e+00	0.000000e+00
Fe II 2609	–4.290130e+04	3.423995e+04	–1.540460e+03	–9.101116e+03	8.113314e+02	0.000000e+00	8.056931e+02	–1.065136e+02	0.000000e+00	–1.165127e-01
	2.225659e+02	–1.009843e+02	0.000000e+00	1.145332e+01	0.000000e+00	0.000000e+00	0.000000e+00	0.000000e+00	0.000000e+00	0.000000e+00
Mg II	–8.369101e+03	4.425491e+03	0.000000e+00	–0.584735e+03	2.583200e+00	0.000000e+00	0.000000e+00	0.000000e+00	–0.426400e+00	0.000000e+00
	4.220988e+02	–1.924251e+02	0.000000e+00	2.195847e+01	0.000000e+00	0.000000e+00	0.000000e+00	0.000000e+00	0.000000e+00	0.000000e+00
Mg I	–6.560245e+04	5.213871e+04	5.667943e+00	–1.379378e+04	0.000000e+00	–7.080052e-01	1.214714e+03	0.000000e+00	0.000000e+00	0.000000e+00
	2.833468e+02	–1.290402e+02	0.000000e+00	1.467496e+01	0.000000e+00	0.000000e+00	0.000000e+00	0.000000e+00	0.000000e+00	0.000000e+00
Mg_{wide}	1.493626e+03	–7.013927e+02	0.000000e+00	8.260315e+01	0.000000e+00	0.000000e+00	0.000000e+00	0.000000e+00	0.000000e+00	0.000000e+00
Fe I	–2.324729e+05	1.873365e+05	–2.620267e+03	–5.027795e+04	1.396493e+03	–1.061878e+00	4.494049e+03	–1.854398e+02	0.000000e+00	0.000000e+00
	1.522971e-02	0.000000e+00	0.000000e+00	0.000000e+00	0.000000e+00	0.000000e+00	0.000000e+00	0.000000e+00	0.000000e+00	0.000000e+00
BL_{3096}	1.153169e+03	–8.051949e+02	0.000000e+00	1.870753e+02	0.000000e+00	0.000000e+00	–1.449478e+01	1.972870e-01	–3.151360e-01	1.554005e-01

Table B.1. Equivalent widths and estimated errors (both in Å) of far-*UV* indices as measured in the IUE spectra of LMC globular clusters.

Cluster	BL_{1302}		Si IV		BL_{1425}		Fe V		C^A_{IV}		C IV		C^E_{IV}		BL_{1617}		BL_{1664}		BL_{1719}		BL_{1853}	
NGC 2011	3.9	0.8	3.5	0.7	0.9	0.7	–0.6	1.1	4.1	0.6	4.1	0.6	2.7	0.6	1.8	0.8	1.1	0.8	1.8	0.6	1.1	0.9
NGC 1805	5.1	0.6	2.5	0.7	1.2	1.7	–0.5	1.1	1.8	0.8	1.7	0.7	0.9	0.8	–0.7	1.1	–0.3	0.8	1.2	0.6	1.0	0.5
NGC 1984	3.9	1.0	4.2	0.9	1.6	1.0	1.0	1.5	2.1	1.1	2.4	1.0	1.2	1.1	1.8	1.5	0.5	1.5	1.5	1.3	1.5	1.6
NGC 2100	3.9	0.4	3.4	0.4	0.3	0.5	–0.9	–0.7	1.8	0.5	2.1	0.5	1.7	0.4	1.7	0.5	1.8	0.5	1.8	0.5	1.4	0.6
NGC 2004	4.2	0.3	3.7	0.4	0.6	0.4	–1.0	0.6	2.9	0.4	2.8	1.5	0.4	0.4	0.9	0.5	0.1	0.6	1.9	0.4	1.4	0.6
NGC 1818	3.8	0.9	1.6	0.8	0.4	0.8	–1.7	1.1	1.2	0.9	1.4	0.7	1.6	0.7	0.9	1.1	0.9	1.2	1.5	1	1.2	1.0
NGC 1847	4.5	0.6	2.8	0.6	0.9	0.7	–0.7	1.0	1.4	0.7	2.5	0.6	1.6	0.7	0.9	0.9	0.8	0.8	1.0	0.6	2.0	0.6
NGC 1711	4.1	0.4	1.8	0.5	–0.3	0.5	–0.9	0.7	1.5	0.5	1.6	0.4	0.9	0.5	0.8	0.6	1.6	0.5	1.4	0.4	1.0	0.4
NGC 1866	4.1	0.7	0.3	0.7	–0.1	0.7	–2.3	1.2	0.4	0.6	0.5	0.5	0.8	0.6	1.2	0.7	1.8	0.6	1.8	0.4	1.9	0.6
NGC 1850	4.4	0.5	0.8	0.6	–0.3	0.6	–2.1	1.0	1.7	0.6	1.4	0.6	1.9	0.6	1.2	0.7	1.1	0.6	1.5	0.4	1.8	0.3

Table B.2. Same as B.1 for mid-*UV* indices.

Cluster	Fe II 2402		BL_{2538}		Fe II2609		Mg II2800		Mg I2852		Mg_{wide}		Fe I3000		BL_{3096}	
NGC 2011	2.9	0.7	0.9	0.5	1.4	0.3	6.0	0.6	0.5	0.7	4.4	2.6	–1.2	1.2	–0.4	0.3
NGC 1805	3.9	2.0	0.3	1.7	2.0	1.2	5.5	1.1	1.0	1.2	7.7	9.3	3.2	3.2	–2.1	2.2
NGC 1984	3.7	1.5	–0.8	1.1	1.6	0.6	3.6	0.5	1.5	0.4	–2.1	4.8	1.0	1.3	–0.3	0.6
NGC 2100	2.1	1.9	–2.5	1.5	0.9	0.9	6.9	0.9	2.4	1.1	0.3	8.1	1.1	3.0	–0.0	1.4
NGC 2004	0.8	0.8	–1.3	0.8	1.3	0.6	6.2	0.6	2.0	0.6	12.7	4.2	0.3	1.3	–0.7	0.6
NGC 1818	1.5	1.3	–0.7	1.1	1.2	0.7	4.9	0.6	1.6	0.7	6.2	5.5	0.0	1.5	0.1	1.0
NGC 1847	1.6	1.7	–1.3	1.1	1.4	0.7	4.7	0.6	1.4	0.6	3.6	5.1	–2.1	1.9	–1.3	0.9
NGC 1711	2.2	1.5	–1.2	1.4	1.6	0.9	6.1	0.8	1.8	0.9	4.1	6.8	2.7	2.2	–1.1	1.3
NGC 1866	2.4	1.6	–0.1	1.4	2.0	0.9	7.1	0.5	2.4	0.5	12	5.2	1.4	1.4	–0.8	1.0
NGC 1850	0.7	1.8	–2.7	1.5	1.2	0.9	6.1	0.9	2.8	0.9	8.6	7.1	0.1	2.5	–1.4	1.5

Appendix C: Age and metallicity estimates of LMC globular clusters based on model line-indices

Table C.1. Ages and metallicities derived from 7 empirical model indices and from 11 Kurucz-based model indices as discussed in Sect. 6 (see Figs. 14 and 15).

Cluster	log(age) (literature)	[Z/H]	log(age) empirical models	[Z/H]	log(age) Kurucz-based models	[Z/H]
NGC 1711	7.70	–0.57	7.10	–1.00	7.50	–0.10
NGC 1805	7.00	–0.20	7.33	–0.33	7.20	–0.33
NGC 1818	7.40	–0.20	7.15	–1.00	7.50	–0.20
NGC 1847	7.42	–0.37	7.10	–0.60	6.85	–0.40
NGC 1850	7.40	–0.12	7.10	–1.00	8.00	–0.10
NGC 1866	8.12	–0.50	8.25	0.10	8.00	–0.50
NGC 1984	7.06	–0.90	6.95	–0.60	7.10	–0.10
NGC 2004	7.30	–0.56	6.95	–0.50	7.20	0.00
NGC 2011	6.99	–0.47	6.80	–0.33	6.70	0.00
NGC 2100	7.20	–0.32	7.00	–0.60	7.35	0.20

References

Alexander, J. B. 1967, MNRAS, 137, 41
Beasley, M. A., Hoyle, F., & Sharples, R. M. 2002, MNRAS, 336, 168
Bell, R. A., & Rodgers, A. W. 1965, MNRAS, 129, 127
Bertelli, G., Bressan, A., Chiosi, C., Fagotto, F., & Nasi, E. 1994, A&AS, 106, 275
Boesgaard, A. M. 1989, ApJ, 336, 798
Boesgaard, A. M., & Friel, E. D. 1990, ApJ, 351, 467
Bonatto, C., Bica, E., & Alloin, D. 1995, A&AS, 112, 71
Bruzual, A. G., & Charlot, S. 1993, ApJ, 405, 538
Bruzual, G., & Charlot, S. 2003, MNRAS, 344, 1000
Burstein, D., Faber, S. M., Gaskell, C. M., & Krumm, N. 1984, ApJ, 287, 586
Burstein, D., Bertola, F., Buson, L. M., Faber, S. M., & Lauer, T. R. 1988, ApJ, 328, 440
Buzzoni, A. 1989, ApJS, 71, 817
Buzzoni, A., Gariboldi, G., & Mantegazza, L. 1992, AJ, 103, 1814
Cardiel, N., Gorgas, J., Cenarro, J., & Gonzalez, J. J. 1998, A&AS, 127, 597
Cassatella, A., Barbero, J., & Geyer, E. H. 1987, ApJS, 64, 83
Castellani, V., Chieffi, A., & Straniero, O. 1992, ApJS, 78, 517
Castelli, F., Cornachin, M., Morossi, C., & Hack, M. 1984, A&A, 141, 223
Cayrel, R., Cayrel de Strobel, G., & Campbell, B. 1985, A&A, 146, 249
Cayrel de Strobel, G., Chauve-Godard, J., Hernandez, G., & Vaziaga, M. J. 1970, A&A, 7, 408
Cayrel de Strobel, G., Soubiran, C., Friel, E. D., Ralite, N., & Francois, P. 1997, A&AS, 124, 299
Cenarro, A. J., Gorgas, J., Cardiel, N., Vazdekis, A., & Peletier, R. F. 2002, MNRAS, 329, 863
Chaffee, Jr., F. H., Carbon, D. F., & Strom, S. E. 1971, ApJ, 166, 593
Chavez, M., Bertone, E., Buzzoni, A., et al. 2007, ApJ, 657, 1046
Cimatti, A., Daddi, E., Renzini, A., et al. 2004, Nature, 430, 184
Coluzzi, R. 1993, Bulletin d'Information du Centre de Données Stellaires, 43, 7
Conti, P. S., Wallerstein, G., & Wing, R. F. 1965, ApJ, 142, 999
Daddi, E., Renzini, A., Pirzkal, N., et al. 2005, ApJ, 626, 680
de Boer, K. S. 1985, A&A, 142, 321
de Grijs, R., Gilmore, G. F., Johnson, R. A., & Mackey, A. D. 2002, MNRAS, 331, 245
de Jager, C., & Nieuwenhuijzen, H. 1987, A&A, 177, 217
de Mello, D. F., Leitherer, C., & Heckman, T. M. 2000, ApJ, 530, 251
de Mello, D. F., Daddi, E., Renzini, A., et al. 2004, ApJ, 608, L29
Dean, C. A., & Bruhweiler, F. C. 1985, ApJS, 57, 133
Dirsch, B., Richtler, T., Gieren, W. P., & Hilker, M. 2000, A&A, 360, 133
Dorman, B., Rood, R. T., & O'Connell, R. W. 1993, ApJ, 419, 596
Dorman, B., O'Connell, R. W., & Rood, R. T. 1995, ApJ, 442, 105
Elson, R. A. W. 1991, ApJS, 76, 185
Elson, R. A., & Fall, S. M. 1988, AJ, 96, 1383
Faber, S. M., Friel, E. D., Burstein, D., & Gaskell, C. M. 1985, ApJS, 57, 711
Fanelli, M. N., O'Connell, R. W., & Thuan, T. X. 1987, ApJ, 321, 768
Fanelli, M. N., O'Connell, R. W., & Thuan, T. X. 1988, ApJ, 334, 665
Fanelli, M. N., O'Connell, R. W., Burstein, D., & Wu, C. 1990, ApJ, 364, 272
Fanelli, M. N., O'Connell, R. W., Burstein, D., & Wu, C. 1992, ApJS, 82, 197
Fioc, M., & Rocca-Volmerange, B. 1997, A&A, 326, 950
Girardi, L., Bertelli, G., Bressan, A., et al. 2002, A&A, 391, 195
Gorgas, J., Faber, S. M., Burstein, D., et al. 1993, ApJS, 86, 153
Graves, G. J., & Schiavon, R. P. 2008, ArXiv e-prints, 803
Greggio, L., & Renzini, A. 1990, ApJ, 364, 35
Heap, S. R., Brown, T. M., Hubeny, I., et al. 1998, ApJ, 492, L131
Hearnshaw, J. B. 1974, A&A, 36, 191
Heckman, T. M., Robert, C., Leitherer, C., Garnett, D. R., & van der Rydt, F. 1998, ApJ, 503, 646
Helfer, H. L., Wallerstein, G., & Greenstein, J. L. 1960, ApJ, 132, 553
Hill, V., François, P., Spite, M., Primas, F., & Spite, F. 2000, A&A, 364, L19

Howarth, I. D., & Prinja, R. K. 1989, ApJS, 69, 527
Humphreys, R. M., & McElroy, D. B. 1984, ApJ, 284, 565
Jasniewicz, G., & Thevenin, F. 1994, A&A, 282, 717
Johnson, R. A., Beaulieu, S. F., Gilmore, G. F., et al. 2001, MNRAS, 324, 367
Kinney, A. L., Bohlin, R. C., Calzetti, D., Panagia, N., & Wyse, R. F. G. 1993, ApJS, 86, 5
Koleva, M., Prugniel, P., Ocvirk, P., Le Borgne, D., & Soubiran, C. 2008, MNRAS, 385, 1998
Kroupa, P. 2001, MNRAS, 322, 231
Kudritzki, R. P., Pauldrach, A., & Puls, J. 1987, A&A, 173, 293
Lee, H.-C., & Worthey, G. 2005, ApJS, 160, 176
Leitherer, C., & Lamers, H. J. G. L. 1991, ApJ, 373, 89
Leitherer, C., & Heckman, T. M. 1995, ApJS, 96, 9
Leitherer, C., Schaerer, D., Goldader, J. D., et al. 1999, ApJS, 123, 3
Lejeune, T., & Schaerer, D. 2001, A&A, 366, 538
Leonardi, A. J., & Rose, J. A. 2003, AJ, 126, 1811
Lotz, J. M., Ferguson, H. C., & Bohlin, R. C. 2000, ApJ, 532, 830
Luck, R. E. 1979, ApJ, 232, 797
Luck, R. E., & Lambert, D. L. 1981, ApJ, 245, 1018
Mackey, A. D., & Gilmore, G. F. 2003, MNRAS, 338, 85
Maraston, C. 1998, MNRAS, 300, 872
Maraston, C. 2005, MNRAS, 362, 799
Maraston, C., Greggio, L., Renzini, A., et al. 2003, A&A, 400, 823
Massa, D. 1989, A&A, 224, 131
McCarthy, P. J., Le Borgne, D., Crampton, D., et al. 2004, ApJ, 614, L9
Mehlert, D., Seitz, S., Saglia, R. P., et al. 2001, A&A, 379, 96
Meynet, G., Maeder, A., Schaller, G., Schaerer, D., & Charbonnel, C. 1994, A&AS, 103, 97
Moore, C. E. 1952, An ultraviolet multiplet table (NBS Circular, Washington: US Government Printing Office (USGPO))
Morton, D. C. 1975, ApJ, 197, 85
O'Connell, R. W. 1976, ApJ, 206, 370
Oliva, E., & Origlia, L. 1998, A&A, 332, 46
Parker, R., Greenstein, J. L., Helfer, H. L., & Wallerstein, G. 1961, ApJ, 133, 101
Pauldrach, A. W. A., Hoffmann, T. L., & Lennon, M. 2001, A&A, 375, 161
Persson, S. E., Aaronson, M., Cohen, J. G., Frogel, J. A., & Matthews, K. 1983, ApJ, 266, 105
Pettini, M., Steidel, C. C., Adelberger, K. L., Dickinson, M., & Giavalisco, M. 2000, ApJ, 528, 96
Ponder, J. M., Burstein, D., O'Connell, R. W., et al. 1998, AJ, 116, 2297
Popesso, P., Dickinson, M., Nonino, M., et al. 2008, ArXiv e-prints, 802
Proctor, R. N., Forbes, D. A., & Beasley, M. A. 2004, MNRAS, 355, 1327
Renzini, A., & Fusi Pecci, F. 1988, ARA&A, 26, 199
Rix, S. A., Pettini, M., Leitherer, C., et al. 2004, ApJ, 615, 98
Robert, C., Leitherer, C., & Heckman, T. M. 1993, ApJ, 418, 749
Rodríguez-Merino, L. H., Chavez, M., Bertone, E., & Buzzoni, A. 2005, ApJ, 626, 411
Salpeter, E. 1955, ApJ, 121, 161
Schaerer, D., Meynet, G., Maeder, A., & Schaller, G. 1993, A&AS, 98, 523
Schaller, G., Schaerer, D., Meynet, G., & Maeder, A. 1992, A&AS, 96, 269
Schiavon, R. P. 2007, ApJS, 171, 146
Schmidt-Kaler, T. 1982, Intrinsic colors and visual absolute magnitudes (calibration of the MK system), ed. L. H. Aller, I. Appenzeller, B. Baschek, et al., 2, 14
Steidel, C. C., Giavalisco, M., Dickinson, M., & Adelberger, K. L. 1996, AJ, 112, 352
Storchi-Bergmann, T., Calzetti, D., & Kinney, A. L. 1994, ApJ, 429, 572
Thomas, D., Maraston, C., & Bender, R. 2003, MNRAS, 339, 897
Tomkin, J., & Lambert, D. L. 1978, ApJ, 223, 937
Underhill, A. B., Leckrone, D. S., & West, D. K. 1972, ApJ, 171, 63
Vazdekis, A., Casuso, E., Peletier, R. F., & Beckman, J. E. 1996, ApJS, 106, 307
Walborn, N. R., & Panek, R. J. 1984, ApJ, 280, L27
Wallerstein, G. 1962, ApJS, 6, 407
Wallerstein, G., & Helfer, H. L. 1959, ApJ, 129, 347
Welty, D. E., Frisch, P. C., Sonneborn, G., & York, D. G. 1999, ApJ, 512, 636
Worthey, G. 1994a, ApJS, 95, 107
Worthey, G. 1994b, ApJS, 95, 107
Worthey, G., Faber, S. M., & Gonzalez, J. J. 1992, ApJ, 398, 69
Worthey, G., Faber, S. M., Gonzalez, J. J., & Burstein, D. 1994, ApJS, 94, 687
Wu, C.-C., Ake, T. B., Boggess, A., et al. 1983, NASA IUE Newsletter, 22, 1
Wu, C.-C., Crenshaw, D. M., Blackwell, J. H., et al. 1991, NASA IUE Newsletter, 43
Yee, H. K. C., Ellingson, E., Bechtold, J., Carlberg, R. G., & Cuillandre, J.-C. 1996, AJ, 111, 1783